

# Synthesis, Crystal Structure, Electrical Properties, and Electronic Band Structure of $(\text{NH}_y\text{Me}_{4-y})_x[\text{M}(\text{dmit})_2]$ Complexes (M = Ni, Pd, Pt; $\text{dmit}^{2-} = 2\text{-Thioxo-1,3-dithiole-4,5-dithiolato}$ )

Brigitte Pomarède,<sup>1a</sup> Bénédicte Garreau,<sup>1a</sup> Isabelle Malfant,<sup>1a</sup> Lydie Valade,<sup>1a</sup> P. Cassoux,<sup>1a</sup> Jean-Pierre Legros,<sup>1a</sup> Alain Audouard,<sup>1b</sup> Luc Brossard,<sup>1b</sup> Jean-Pierre Ulmet,<sup>1b</sup> Marie-Liesse Doublet,<sup>1c</sup> and Enric Canadell<sup>1c</sup>

Laboratoire de Chimie de Coordination du CNRS lié par convention à l'Université Paul Sabatier de Toulouse, 205 route de Narbonne, 31077 Toulouse Cedex, France, Service National des Champs Magnétiques Pulsés et Laboratoire de Physique des Solides, INSA-Université Paul Sabatier de Toulouse, avenue de Rangueil, 31077 Toulouse Cedex, France, and Laboratoire de Chimie Théorique, Université de Paris-Sud, 91405 Orsay, France

Received October 19, 1993<sup>o</sup>

Seven phases of the family  $(\text{NH}_y\text{Me}_{4-y})_x[\text{M}(\text{dmit})_2]$  (M = Ni, Pd, Pt) have been isolated as single crystals by the electrocrystallization technique:  $(\text{NMe}_4)_{0.5}[\text{Ni}(\text{dmit})_2]$  (1),  $(\text{NHMe}_3)_{0.5}[\text{Ni}(\text{dmit})_2]$  (2),  $(\text{NHMe}_3)_2[\text{Ni}(\text{dmit})_2]_5 \cdot 2\text{MeCN}$  (3),  $(\text{NH}_2\text{Me}_2)_{0.5}[\text{Ni}(\text{dmit})_2]$  (4),  $(\text{NH}_3\text{Me})_2[\text{Ni}(\text{dmit})_2]_5 \cdot 2\text{MeCN}$  (5),  $(\text{NH}_4)_x[\text{Ni}(\text{dmit})_2]$  (6), and  $(\text{NHMe}_3)_{0.5}[\text{Pt}(\text{dmit})_2]_3 \cdot \text{MeCN}$  (7). All these phases are built of stacked  $\text{M}(\text{dmit})_2$  entities forming anionic slabs which alternate with sheets containing the cations (and the solvent molecules when present). In phases 1, 2, and 4 the  $\text{Ni}(\text{dmit})_2$  entities are paired and form weak dimers. Phases 1 and 2 are highly conductive:  $\sigma_{\text{RT}} = 55$  and  $140 \text{ S}\cdot\text{cm}^{-1}$ , respectively. At ambient pressure a metal-like temperature-dependent behavior is observed down to 90 and 220 K respectively. Under pressure the superconducting transition reported previously for 1 is not observed; nonohmic behavior is observed at low temperature. Comparison of the crystal and electronic band structures of 1 and 2 indicates that the nature of the pseudometal-to-insulator transition of 1 cannot result from a CDW instability while such an instability cannot be ruled out in 2. Phase 4 is semiconductive ( $\sigma_{\text{RT}} = 0.1 \text{ S}\cdot\text{cm}^{-1}$ ;  $E_a = 0.21 \text{ eV}$ ). Phases 3 and 5 are also semiconductive ( $\sigma_{\text{RT}} = 0.2$  and  $1.5 \text{ S}\cdot\text{cm}^{-1}$ ;  $E_a = 0.23$  and  $0.20 \text{ eV}$ ). In these phases with 2:5 stoichiometry, the repeating unit of a stack is made of two weak dimers and one single molecule; tight-binding band structure calculations suggest that the two electrons are localized on the two weak dimers while the single molecule is neutral. All samples of 6 are found to be semiconductive ( $\sigma_{\text{RT}} = 0.2\text{--}0.7 \text{ S}\cdot\text{cm}^{-1}$  in agreement with previous work); the metallic phase of 6 described by other authors is not found. The conductivity of phase 7 ( $\sigma_{\text{RT}} = 140 \text{ S}\cdot\text{cm}^{-1}$ ) is the highest observed in  $\text{Pt}(\text{dmit})_2$  compounds; it remains almost constant down to 180 K and then drops sharply. The crystal structure of 7 is made of stacks of  $[\text{Pt}(\text{dmit})_2]_2$  dimers characterized by strong Pt-Pt interactions. In contrast to 1 and 2 where intrastack interactions are predominant, band structure calculations for 7 indicate the dominant character of the interstack interactions in the conduction process.

## Introduction

Among the *ca.* 70 compounds derived from the metal complexes of the dmit ligand ( $\text{dmit}^{2-} = 2\text{-thioxo-1,3-dithiole-4,5-dithiolato}$ ; Figure 1),<sup>2</sup> a number of molecular metals and seven superconducting phases,<sup>3</sup> including the ambient pressure superconducting  $\alpha\text{-(EDT-TTF)[Ni}(\text{dmit})_2]$ ,<sup>4</sup> have been characterized. They form the first and unique series of molecular inorganic superconductors. In addition to superconductivity, these systems exhibit interesting electrical properties, such as original pressure dependence of the critical temperature<sup>5</sup> and the presence of charge density wave (CDW) states,<sup>6</sup> which, in some cases, do not induce a metal-to-insulator transition,<sup>7</sup> these properties being related to a unique multisheet band structure.<sup>8</sup>

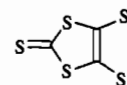


Figure 1. The  $\text{dmit}^{2-}$  ligand.

In the series of anion radical salts  $(\text{NR}_4)_{0.5}[\text{M}(\text{dmit})_2]$ , the tetramethylammonium counteranion is common to the two superconducting phases  $(\text{NMe}_4)_{0.5}[\text{Ni}(\text{dmit})_2]$ <sup>9</sup> and  $\beta\text{-(NMe}_4)_{0.5}[\text{Pd}(\text{dmit})_2]$ <sup>10</sup> whereas larger tetraalkylammonium cations (R = Et, Bu), lead usually to semiconducting systems.<sup>11,12</sup> However, the intermediate mixed  $(\text{NMe}_2\text{Et}_2)_{0.5}[\text{Pd}(\text{dmit})_2]$  compound is also superconducting.<sup>13</sup> Following a straightforward strategy involving the use of smaller  $\text{NMe}_4$ -derived cations, we have started a systematic study of the  $(\text{NH}_y\text{Me}_{4-y})_x[\text{M}(\text{dmit})_2]$  series of

<sup>o</sup> Abstract published in *Advance ACS Abstracts*, June 1, 1994.

- (a) Laboratoire de Chimie de Coordination. (b) Service National des Champs Magnétiques Pulsés et Laboratoire de Physique des Solides. (c) Laboratoire de Chimie Théorique.
- Cassoux, P.; Valade, L.; Kobayashi, H.; Kobayashi, A.; Clark, R. A.; Underhill, A. E. *Coord. Chem. Rev.* **1991**, *110*, 115–160.
- Cassoux, P.; Valade, L. In *Inorganic Materials*; Bruce, D. W., O'Hare, D., Eds.; John Wiley & Sons Ltd.: Chichester, England, 1991; pp 1–58.
- Tajima, H.; Inokuchi, M.; Kobayashi, A.; Ohta, T.; Kato, R.; Kobayashi, H.; Kuroda, H. *Chem. Lett.* **1993**, 1235–1238.
- Brossard, L.; Ribault, M.; Valade, L.; Cassoux, P. *Phys. Rev. B* **1990**, *42*, 3935–3943.
- Ravy, S.; Pouget, J.-P.; Valade, L.; Legros, J.-P. *Europhys. Lett.* **1989**, *9*, 391–396. Ravy, S.; Canadell, E.; Pouget, J.-P. In *The Physics and Chemistry of Organic Superconductors*; Saito, G., Kagoshima, S., Eds.; Springer Proceedings in Physics 51; Springer Verlag: Berlin, 1990, pp 252–256.

- Brossard, L.; Ribault, M.; Valade, L.; Cassoux, P. *C. R. Acad. Sci. (Paris) Sér. 2* **1989**, *309*, 1117–1123.
- Canadell, E.; Ravy, S.; Pouget, J.-P.; Brossard, L. *Solid State Commun.* **1990**, *75*, 633–638.
- Kobayashi, A.; Kim, H.; Sasaki, Y.; Kato, R.; Kobayashi, H.; Moriyama, S.; Nishio, Y.; Kajita, K.; Sasaki, W. *Chem. Lett.* **1987**, 1819–1822. Kajita, K.; Nishio, Y.; Moriyama, S.; Kato, R.; Kobayashi, H.; Sasaki, W.; Kobayashi, A.; Kim, H.; Sasaki, Y. *Solid State Commun.* **1988**, *65*, 361–363.
- Kobayashi, A.; Kobayashi, H.; Miyamoto, A.; Kato, R.; Clark, R. A.; Underhill, A. E. *Chem. Lett.* **1991**, 2163–2166.
- Kato, R.; Mori, T.; Kobayashi, A.; Sasaki, Y.; Kobayashi, H. *Chem. Lett.* **1984**, 1–4.
- Valade, L.; Legros, J.-P.; Bousseau, M.; Cassoux, P.; Garbauskas, M.; Interrante, L. V. *J. Chem. Soc., Dalton Trans.* **1985**, 783–794.

**Table 1.** Electrocrystallization Conditions of Seven Characterized  $(\text{NH}_y\text{Me}_{4-y})_x[\text{M}(\text{dmit})_2]$  Anion Radical Salts

starting complex	solvent	electrolyte	intensity, $\mu\text{A}$	phase obtained
$(\text{NMe}_4)[\text{Ni}(\text{dmit})_2]$	MeCN	$(\text{NMe}_4)\text{Br}$	0.6	$(\text{NMe}_4)_{0.5}[\text{Ni}(\text{dmit})_2]$ (1)
$(\text{NHMe}_3)[\text{Ni}(\text{dmit})_2]$	MeCN	$(\text{NHMe}_3)\text{BF}_4$	1	$(\text{NHMe}_3)_{0.5}[\text{Ni}(\text{dmit})_2]$ (2)
$(\text{NHMe}_3)[\text{Ni}(\text{dmit})_2]$	MeCN <sup>a</sup>	$(\text{NHMe}_3)\text{BF}_4$	1	$(\text{NHMe}_3)_2[\text{Ni}(\text{dmit})_2]_2 \cdot 2\text{MeCN}$ (3)
$(\text{NH}_2\text{Me}_2)[\text{Ni}(\text{dmit})_2]$	MeCN	$(\text{NH}_2\text{Me}_2)\text{BPh}_4$	1	$(\text{NH}_2\text{Me}_2)_{0.5}[\text{Ni}(\text{dmit})_2]$ (4)
$(\text{NH}_3\text{Me})[\text{Ni}(\text{dmit})_2]$	MeCN	$(\text{NH}_3\text{Me})\text{BF}_4$	1	$(\text{NH}_3\text{Me})_2[\text{Ni}(\text{dmit})_2]_2 \cdot 2\text{MeCN}$ (5)
$(\text{NBu}_4)[\text{Ni}(\text{dmit})_2]$	$\text{MeNO}_2/\text{Me}_2\text{CO}^b$	$(\text{NH}_4)\text{BF}_4^c$	1	$(\text{NH}_4)_x[\text{Ni}(\text{dmit})_2]$ (6)
$(\text{NHMe}_3)[\text{Pt}(\text{dmit})_2]$	MeCN/EtOH <sup>d</sup>	$(\text{NHMe}_3)\text{BF}_4$	1	$(\text{NHMe}_3)[\text{Pt}(\text{dmit})_2]_3 \cdot \text{MeCN}$ (7)

<sup>a</sup> 1% H<sub>2</sub>O. <sup>b</sup> 50/50%. <sup>c</sup> 20-fold excess with respect to  $(\text{NBu}_4)[\text{Ni}(\text{dmit})_2]$ . <sup>d</sup> 90/10%.

compounds with  $y = 0, 1, 2, 3,$  and  $4$  and  $\text{M} = \text{Ni}, \text{Pd},$  and  $\text{Pt}$ . We report in this paper the synthesis of these compounds, their electrochemical behavior, and the crystal structure, electrical properties, and electronic band structure of the most interesting ones. Some preliminary reports have appeared on this subject.<sup>14–16</sup>

### Experimental Section

**Syntheses.** All syntheses were carried out using vacuum line and Schlenk techniques in dried N<sub>2</sub> atmosphere. The main starting compounds,  $(\text{NBu}_4)_2[\text{Zn}(\text{dmit})_2]$ ,<sup>12,17</sup>  $\text{dmit}(\text{COPh})_2$ ,<sup>12,17</sup> and  $\text{dmitNa}_2$ ,<sup>18</sup> and the  $(\text{NMe}_4)_{0.5}[\text{Ni}(\text{dmit})_2]$ <sup>9</sup> and  $(\text{NH}_4)_x[\text{Ni}(\text{dmit})_2]$ <sup>19</sup> compounds, have been prepared as previously described.

**$(\text{NHMe}_3)_2[\text{M}(\text{dmit})_2]$  and  $(\text{NH}_2\text{Me}_2)_2[\text{M}(\text{dmit})_2]$  Complexes.** These divalent complexes have been prepared from  $\text{dmit}(\text{COPh})_2$  following a procedure inspired from that previously used in the preparation of  $(\text{NR}_4)_2[\text{M}(\text{dmit})_2]$ <sup>12,17</sup> but involving the addition of an excess of the  $(\text{NHMe}_3)\text{Cl}$  or  $(\text{NH}_2\text{Me}_2)\text{Cl}$  precipitating reagent respectively (method of excess *E*; see Discussion). For example, the synthesis of  $(\text{NHMe}_3)_2[\text{Pt}(\text{dmit})_2]$  has been previously described.<sup>15</sup> The nickel and palladium  $(\text{NHMe}_3)_2[\text{M}(\text{dmit})_2]$  analogs and the  $(\text{NH}_2\text{Me}_2)_2[\text{M}(\text{dmit})_2]$  complexes ( $\text{M} = \text{Ni}, \text{Pd}, \text{Pt}$ ) can be obtained in a similar way when using the appropriate metal salt,  $\text{K}_2\text{PtCl}_4$ ,  $\text{NiCl}_2 \cdot 6\text{H}_2\text{O}$ , and  $\text{Na}_2\text{PdCl}_4 \cdot 3\text{H}_2\text{O}$ , respectively.<sup>20</sup>

**$(\text{NH}_3\text{Me})_2[\text{M}(\text{dmit})_2]$  Complexes.** These divalent complexes have been prepared (method of isolation *I*; see Discussion) from the  $\text{dmitNa}_2$  salt which should be isolated in a first step.<sup>18,20</sup> Typically, to a solution of  $\text{dmitNa}_2$  (7.38 mmol in 20 mL of methanol) is added a solution of  $\text{NiCl}_2 \cdot 6\text{H}_2\text{O}$  (3.21 mmol in 50 mL of methanol) and the mixture is stirred for 1 h at room temperature. To the resulting violet solution is added a solution of  $(\text{NH}_3\text{Me})\text{Cl}$  (7.6 mmol in 30 mL of methanol). After 1 h of stirring, the solution is evaporated under vacuum to dryness. The resulting solid residue is dissolved in acetonitrile (250 mL) and the obtained solution is filtered and evaporated again to 100 mL. The  $(\text{NH}_3\text{Me})_2[\text{Ni}(\text{dmit})_2]$  complex is precipitated by addition of 100 mL of diethyl ether, filtered off, washed with diethyl ether, and dried under vacuum (yield 90%). It should be noted that the  $(\text{NH}_2\text{Me}_2)_2[\text{M}(\text{dmit})_2]$  complexes could be also obtained following method *I*. The  $(\text{NH}_4)_2[\text{M}(\text{dmit})_2]$  complexes could not be obtained using either method *E* or method *I*.

**$(\text{NH}_y\text{Me}_{4-y})[\text{M}(\text{dmit})_2]$  Complexes.** All these monovalent complexes with  $y = 1, 2,$  and  $3$  and  $\text{M} = \text{Ni}, \text{Pd},$  and  $\text{Pt}$  were obtained from the corresponding divalent  $(\text{NH}_y\text{Me}_{4-y})_2[\text{M}(\text{dmit})_2]$  complexes by oxidation with  $\text{I}_2/\text{NaI}$ , or by air oxidation in the presence of acetic acid, following previously reported procedures.<sup>17,20</sup> The  $(\text{NH}_4)[\text{M}(\text{dmit})_2]$  complexes can be directly prepared by redissolving in acetone the intermediate solid residue obtained after evaporation to dryness following method *I* (*vide supra*), and oxidizing the resulting solution with  $\text{I}_2/\text{NaI}$ . However, the yields are extremely low.<sup>20</sup>

**Table 2.** Crystallographic Data for  $(\text{NHMe}_3)[\text{Ni}(\text{dmit})_2]_2$  (2),  $(\text{NHMe}_3)_2[\text{Ni}(\text{dmit})_2]_2 \cdot 2\text{MeCN}$  (3) and  $(\text{NH}_2\text{Me}_2)_{0.5}[\text{Ni}(\text{dmit})_2]$  (4)

	2	3	4
chem formula	$\text{Ni}_2\text{C}_{15}\text{H}_{10}\text{NS}_{20}$	$\text{Ni}_5\text{C}_{40}\text{H}_{26}\text{N}_4\text{S}_{50}$	$\text{Ni}_2\text{C}_{14}\text{H}_8\text{NS}_{20}$
fw	963.0	2459.4	948.8
space group	$P\bar{1}$	$P\bar{1}$	$P\bar{1}$
<i>a</i> , Å	7.535(1)	18.205(2)	7.513(1)
<i>b</i> , Å	17.558(2)	19.472(2)	16.137(2)
<i>c</i> , Å	6.623(1)	6.506(4)	6.527(2)
$\alpha$ , deg	100.61(1)	92.21(2)	92.83(2)
$\beta$ , deg	113.88(1)	98.04(2)	109.10(2)
$\gamma$ , deg	87.37(1)	63.72(1)	92.23(1)
<i>V</i> , Å <sup>3</sup>	787(3)	2047(1)	746(5)
$\rho_{\text{calcd}}$ , g cm <sup>-3</sup>	2.03	2.00	2.11
<i>Z</i>	1	1	1
$\mu(\text{Mo K}\alpha)$ , cm <sup>-1</sup>	25.0	24.0	26.3
<i>T</i> , °C	20	20	20
<i>R</i> ( <i>F</i> <sub>o</sub> ) <sup>a</sup>	0.061	0.041	0.020
<i>R</i> <sub>w</sub> ( <i>F</i> <sub>o</sub> ) <sup>a</sup>	0.071	0.039	0.036

<sup>a</sup>  $R(F_o) = \sum(|F_o| - |F_c|) / \sum F_o$  and  $R_w(F_o) = [\sum w(|F_o| - |F_c|)^2 / \sum w F_o^2]^{1/2}$ .

All above mentioned compounds gave satisfactory elemental analyses and the expected IR spectra.<sup>20</sup>

**$(\text{NH}_y\text{Me}_{4-y})_x[\text{M}(\text{dmit})_2]$  Anion Radical Salts.** All these salts with  $y = 1, 2,$  and  $3$  and  $\text{M} = \text{Ni}, \text{Pd},$  and  $\text{Pt}$  have been obtained by galvanostatic oxidation of a solution of the corresponding  $(\text{NH}_y\text{Me}_{4-y})[\text{M}(\text{dmit})_2]$  complexes using previously described techniques.<sup>3</sup> In many cases, powders or poor quality crystals have been obtained on the anode. However, crystals of suitable size and quality have been obtained in six cases (Table 1) and have been characterized by X-ray diffraction methods.

Not having at our disposal sizable quantities of the  $(\text{NH}_4)[\text{M}(\text{dmit})_2]$  precursor complexes, the corresponding  $(\text{NH}_4)_x[\text{M}(\text{dmit})_2]$  have been prepared by following a previously described procedure,<sup>19</sup> by electrocrystallization of solutions of  $(\text{NBu}_4)[\text{M}(\text{dmit})_2]$  in the presence of a very large excess of  $(\text{NH}_4)\text{Cl}$ .

**Electrochemical Studies.** Voltammetric measurements and controlled potential electrolyses were carried out using previously described apparatus and techniques.<sup>16,21</sup>

**X-ray Diffraction Data Collections and Structure Determinations.** All data were collected at room temperature on an Enraf-Nonius CAD4 diffractometer with graphite-monochromated Mo K $\alpha$  radiation ( $\lambda = 0.71073$  Å) using the  $\omega$ - $2\theta$  scan mode. Accurate unit cell parameters were obtained by least-squares refinements based on the setting angles of 25 reflections. Crystallographic data for  $(\text{NHMe}_3)_{0.5}[\text{Ni}(\text{dmit})_2]$  (2),  $(\text{NHMe}_3)_2[\text{Ni}(\text{dmit})_2]_2 \cdot 2\text{MeCN}$  (3),<sup>22</sup>  $(\text{NH}_2\text{Me}_2)_{0.5}[\text{Ni}(\text{dmit})_2]$  (4),  $(\text{NH}_3\text{Me})_2[\text{Ni}(\text{dmit})_2]_2 \cdot 2\text{MeCN}$  (5)<sup>22</sup> and  $(\text{NHMe}_3)[\text{Pt}(\text{dmit})_2]_3 \cdot \text{MeCN}$  (7),<sup>22</sup> respectively, are summarized in Tables 2 and 3; relevant parameters of data collections and refinements are given in supplementary material (Tables S1 and S2). In all cases, the intensity of three reflections was monitored throughout the data collection and no significant decay was observed; empirical absorption corrections were applied. The structures were solved by direct method;<sup>23</sup> and refined using standard full-matrix least-squares and Fourier procedures.<sup>24</sup> All non-hydrogen atoms were refined anisotropically [for compound 5 atoms of the disordered  $(\text{NH}_3\text{Me})^+$  cation and of the MeCN solvent molecule were refined isotropically]. For the nonordered structures, hydrogen atoms which could be located

- (13) Kobayashi, H.; Bun, K.; Naito, T.; Kato, R.; Kobayashi, A. *Chem. Lett.* **1992**, 1909–1912. Kobayashi, A.; Kato, R.; Clark, R. A.; Underhill, A. E.; Miyamoto, A.; Bun, K.; Naito, T.; Kobayashi, H. *Synth. Met.* **1993**, 55–57, 2927–2932.
- (14) Tejel, C.; Pomarède, B.; Legros, J.-P.; Valade, L.; Cassoux, P.; Ulmet, J.-P. *Chem. Mater.* **1989**, *1*, 578–580.
- (15) Garreau, B.; Pomarède, B.; Cassoux, P.; Legros, J.-P. *J. Mater. Chem.* **1993**, *3*, 315–316.
- (16) Tommasino, J.-B.; Pomarède, B.; Medus, D.; de Montauzon, D.; Cassoux, P. *Mol. Cryst. Liq. Cryst.*, in press.
- (17) Steimecke, G.; Sieler, H. J.; Kirmse, R.; Hoyer, E. *Phosphorus Sulfur* **1979**, *7*, 49–55. Hartke, K.; Kissel, T.; Quante, J.; Matusch, R. *Chem. Ber.* **1980**, *113*, 1898–1906.
- (18) Varma, K. S.; Bury, A.; Harris, N. J.; Underhill, A. E. *Synthesis* **1987**, *9*, 837–838.
- (19) Izuoka, A.; Miyazaki, A.; Sato, N.; Sugawara, T.; Enoki, T. In *The Physics and Chemistry of Organic Superconductors* Saito, G., Kagoshima, S., Eds.; Springer Proceedings in Physics 51; Springer Verlag: Berlin, 1990, pp 32–35.
- (20) Pomarède, B. Ph.D. Thesis, Toulouse, France 1992.

- (21) Faulmann, C.; Cassoux, P.; Yagubskii, E. B.; Vetoshkina, L. V. *New J. Chem.* **1993**, *17*, 385–391.
- (22) The  $[\text{cation}]_x[\text{M}(\text{dmit})_2]$  formula writing evidences the nonintegral oxidation state ( $x < 1$ ) in these complexes. In some cases, especially for compounds involving crystallization solvent molecules, the  $[\text{cation}]_x[\text{M}(\text{dmit})_2]_m(\text{solvent})_p$  formula writing has been used.
- (23) Sheldrick, G. M. *SHELX 86, Program for Crystal Structure Solution*; University of Göttingen: Göttingen, Germany 1986.
- (24) Fair, C. K. *MOLÉN, Structure Determination System*; Enraf-Nonius: Delft, The Netherlands, 1990.

**Table 3.** Crystallographic Data for (NH<sub>3</sub>Me)<sub>2</sub>[Ni(dmit)<sub>2</sub>]<sub>5</sub>·2MeCN (5) and (NHMe<sub>3</sub>)<sub>2</sub>[Pt(dmit)<sub>2</sub>]<sub>3</sub>·MeCN (7)

	(5)	(7)
chem formula	Ni <sub>5</sub> C <sub>36</sub> H <sub>18</sub> N <sub>4</sub> S <sub>30</sub>	Pt <sub>3</sub> C <sub>22</sub> H <sub>13</sub> N <sub>2</sub> S <sub>30</sub>
fw	2403.3	1854.6
space group	P $\bar{1}$	P $\bar{1}$
a, Å	18.329(2)	17.607(3)
b, Å	19.426(2)	18.509(4)
c, Å	6.523(3)	7.797(3)
$\alpha$ , deg	91.05(3)	93.54(2)
$\beta$ , deg	97.20(4)	98.34(2)
$\gamma$ , deg	64.61(2)	107.96(2)
V, Å <sup>3</sup>	2080(1)	2376(1)
$\rho_{\text{calc}}$ , g cm <sup>-3</sup>	1.92	2.61
Z	1	2
$\mu$ (Mo K $\alpha$ ), cm <sup>-1</sup>	23.6	102.0
T, °C	20	20
R(F <sub>o</sub> ) <sup>a</sup>	0.050	0.033
R <sub>w</sub> (F <sub>o</sub> ) <sup>a</sup>	0.057	0.037

$$^a R(F_o) = \sum(|F_o| - |F_c|) / \sum|F_o| \text{ and } R_w(F_o) = [\sum w(|F_o| - |F_c|)^2 / \sum w F_o^2]^{1/2}.$$

**Table 4.** Atomic Parameters for (NHMe<sub>3</sub>)<sub>0.5</sub>[Ni(dmit)<sub>2</sub>] (2)

atom	x/a	y/b	z/c	B <sub>eq</sub> <sup>a</sup> , Å <sup>2</sup>
Ni	0.26520(5)	0.46830(2)	0.50514(6)	2.449(8)
S(1)	0.2553(1)	0.40277(5)	0.1895(1)	2.94(2)
S(2)	0.3369(1)	0.36884(5)	0.6695(1)	3.08(2)
S(3)	0.3186(1)	0.23190(6)	0.0571(2)	3.45(2)
S(4)	0.3966(1)	0.20239(5)	0.4997(2)	3.39(2)
S(5)	0.4095(2)	0.07164(6)	0.1511(2)	5.03(3)
S(6)	0.1968(1)	0.57067(5)	0.3512(1)	3.02(2)
S(7)	0.2696(1)	0.53023(5)	0.8197(1)	3.01(2)
S(8)	0.1497(1)	0.73706(5)	0.5438(2)	3.25(2)
S(9)	0.2173(1)	0.69866(5)	0.9752(1)	3.07(2)
S(10)	0.1555(2)	0.86203(6)	0.9199(2)	4.42(2)
C(1)	0.3094(4)	0.3117(2)	0.2524(5)	2.66(6)
C(2)	0.3446(4)	0.2973(2)	0.4611(5)	2.70(6)
C(3)	0.3757(5)	0.1640(2)	0.2314(6)	3.43(8)
C(4)	0.1940(4)	0.6398(2)	0.5658(5)	2.52(6)
C(5)	0.2257(4)	0.6219(2)	0.7714(5)	2.53(6)
C(6)	0.1722(4)	0.7706(2)	0.8164(6)	3.07(7)
N <sup>b</sup>	0.927(1)	0.0146(4)	0.435(1)	4.1(2)
C(10) <sup>b</sup>	0.804(2)	-0.0267(8)	0.494(2)	8.3(3)
C(11) <sup>b</sup>	1.067(2)	-0.0371(9)	0.368(2)	8.5(4)
C(12) <sup>b</sup>	1.033(3)	0.0752(8)	0.625(2)	14.4(8)

$$^a B_{\text{eq}} = (4/3) \sum_i \sum_j \beta_i \beta_j. \quad ^b \text{Structure occupation factor 0.5.}$$

on Fourier difference maps were included in structure factor calculations using idealized positional parameters and arbitrary isotropic temperature factor ( $U = 0.07 \text{ \AA}^2$ ). All calculations were performed on a microVAX 3400 DEC computer. Final non-hydrogen atom positional and equivalent thermal parameters are listed in Tables 4–8. The anisotropic thermal parameters are given in the supplementary material (Tables S3–S9). The atomic numbering schemes are shown in Figures 2–4. The atomic scattering factors used were those calculated by Cromer and Waber.<sup>25</sup>

**Conductivity Measurements.** Ambient pressure, room-temperature compacted powder conductivity, temperature dependent (300–4 K) single-crystal conductivity,<sup>26</sup> and pressure dependent conductivity<sup>27</sup> measurements have been carried out as previously described. DC conductivity measurements have been performed on (NHMe<sub>3</sub>)<sub>0.5</sub>[Ni(dmit)<sub>2</sub>] with constant currents ranging from 5 pA to 1 mA. Nonlinear behavior being observed, differential resistance ( $dV/dI$ ) measurements were carried out as usual.<sup>28</sup> Calculations of the dissipated power show that self-heating of the sample is avoided.

**Electronic Band Structure Calculations.** The electronic structures were obtained on the basis of extended Hückel<sup>29</sup> tight-binding (EHTB) band structure calculations.<sup>30a</sup> The off-diagonal matrix elements of the effective Hamiltonian were calculated according to the modified Wolfsberg–Helmholz formula.<sup>30b</sup> The exponents, contraction coefficients and atomic parameters used in the calculations are summarized in Table 9.

(25) Cromer, D. T.; Waber, J. T. *International Tables for X-Ray Crystallography*; Kynoch Press: Birmingham, England, 1974; Vol. IV, Table 2.2B, p 99.

(26) Galy, J.; Enjalbert, R.; Millet, P.; Faulmann, C.; Cassoux, P. *J. Solid State Chem.* **1988**, *74*, 356–358.

(27) Brossard, L.; Ribault, M.; Garreau, B.; Pomarède, B.; Cassoux, P. *Europhys. Lett.* **1992**, *19*, 223–227.

(28) Richard, J.; Monceau, P.; Renard, M. *Phys. Rev. B* **1987**, *35*, 4533–4536.

**Table 5.** Atomic Parameters for (NHMe<sub>3</sub>)<sub>2</sub>[Ni(dmit)<sub>2</sub>]<sub>5</sub>·2MeCN (3)

atom	x/a	y/b	z/c	B <sub>eq</sub> <sup>a</sup> , Å <sup>2</sup>
Ni(1)	1/2	1/2	1/2	2.09(1)
S(11)	0.48174(6)	0.56106(5)	0.7840(2)	2.69(2)
S(12)	0.46767(7)	0.71825(6)	0.8927(2)	3.09(2)
S(13)	0.47293(8)	0.86315(6)	0.7963(2)	3.91(3)
S(14)	0.49200(7)	0.74534(5)	0.4786(2)	3.02(2)
S(15)	0.50323(6)	0.59223(5)	0.3367(1)	2.65(2)
C(11)	0.4805(2)	0.6448(2)	0.7200(6)	2.19(8)
C(12)	0.4769(2)	0.7799(2)	0.7262(6)	2.55(9)
C(13)	0.4907(2)	0.6586(2)	0.5211(6)	2.36(8)
Ni(2)	0.09794(3)	0.53332(3)	0.71473(7)	2.23(1)
S(21)	0.09528(6)	0.43892(5)	0.8728(2)	2.71(2)
S(22)	0.11361(6)	0.28341(5)	0.7213(2)	3.00(2)
S(23)	0.14147(8)	0.16648(6)	0.3914(2)	4.33(3)
S(24)	0.13111(6)	0.31779(5)	0.3078(2)	2.86(2)
S(25)	0.11564(6)	0.47394(5)	0.4273(2)	2.65(2)
S(26)	0.07583(6)	0.59592(5)	0.9989(2)	2.58(2)
S(27)	0.06001(7)	0.75426(6)	1.1029(2)	3.20(2)
S(28)	0.05594(8)	0.90334(6)	1.0022(2)	4.81(3)
S(29)	0.08375(7)	0.78184(5)	0.6902(2)	3.16(2)
S(30)	0.10271(6)	0.62551(5)	0.5511(2)	2.79(2)
C(21)	0.1098(2)	0.3729(2)	0.6856(6)	2.37(8)
C(22)	0.1292(2)	0.2517(2)	0.4708(6)	2.92(9)
C(23)	0.1175(2)	0.3892(2)	0.4859(6)	2.20(8)
C(24)	0.0755(2)	0.6794(2)	0.9320(6)	2.41(8)
C(25)	0.0661(2)	0.8173(2)	0.9350(7)	3.01(9)
C(26)	0.0870(2)	0.6931(2)	0.7364(6)	2.43(8)
Ni(3)	0.30271(3)	0.43684(2)	0.03181(7)	2.12(1)
S(31)	0.28615(6)	0.49909(5)	0.3156(1)	2.60(2)
S(32)	0.27487(6)	0.65583(6)	0.4179(2)	2.88(2)
S(33)	0.27465(8)	0.80265(6)	0.3039(2)	4.61(3)
S(34)	0.29192(6)	0.68320(5)	-0.0033(2)	2.93(2)
S(35)	0.30461(6)	0.52896(5)	-0.1377(1)	2.59(2)
S(36)	0.29695(6)	0.34639(5)	0.2001(1)	2.62(2)
S(37)	0.31329(6)	0.19030(5)	0.0677(2)	2.77(2)
S(38)	0.34925(8)	0.06398(6)	-0.2320(2)	4.21(3)
S(39)	0.34323(6)	0.21252(5)	-0.3427(2)	2.85(2)
S(40)	0.32599(6)	0.37205(5)	-0.2480(1)	2.49(2)
C(31)	0.2857(2)	0.5826(2)	0.2480(6)	2.29(8)
C(32)	0.2806(2)	0.7183(2)	0.2455(6)	2.74(9)
C(33)	0.2933(2)	0.5954(2)	0.0455(6)	2.12(8)
C(34)	0.3124(2)	0.2777(2)	0.0190(6)	2.25(8)
C(35)	0.3358(2)	0.1509(2)	-0.1720(6)	2.71(9)
C(36)	0.3258(2)	0.2886(2)	-0.1784(6)	2.22(8)
N(1)	0.1824(2)	0.0021(2)	0.7006(6)	4.7(1)
C(41)	0.1522(3)	0.0588(3)	0.8616(9)	6.1(2)
C(42)	0.2408(3)	-0.0746(3)	0.7924(9)	6.0(2)
C(43)	0.1137(3)	-0.0023(3)	0.559(1)	6.4(2)
N(3)	0.7134(3)	0.0272(2)	0.6523(7)	5.9(1)
C(51)	0.6532(3)	0.0285(3)	0.6769(7)	4.4(1)
C(52)	0.5749(3)	0.0305(4)	0.7062(8)	6.1(2)

$$^a B_{\text{eq}} = (4/3) \sum_i \sum_j \beta_i \beta_j.$$

## Results and Discussion

**Syntheses and Electrochemical Characterizations.** Most of the divalent (cation)<sub>2</sub>[M(dmit)<sub>2</sub>] complexes previously reported<sup>2</sup> were prepared following the straightforward one-step method<sup>12,17</sup> outlined in Scheme 1: in this method, the dmit<sup>2-</sup> species, stable in strongly basic media, is generated *in situ* by treating dmit-(COPH)<sub>2</sub> with an excess of sodium methanolate.

Whereas this method was successfully applied to the case of the (NR<sub>4</sub>)<sub>2</sub>[M(dmit)<sub>2</sub>] complexes, it failed in the cases of the (NHMe<sub>3</sub>)<sub>2</sub>[M(dmit)<sub>2</sub>] complexes. This results from a side reaction between the excess of methanolate and (NHMe<sub>3</sub>)-Cl (yielding NMe<sub>3</sub>, Scheme 2) which prevents the desired (NHMe<sub>3</sub>)<sub>2</sub>[M(dmit)<sub>2</sub>] complexes from being isolated. Therefore, these complexes were obtained by method E which involves in its last step the use of a very large excess of (NHMe<sub>3</sub>)Cl.<sup>15</sup> The

(29) (a) Hoffmann, R. *J. Chem. Phys.* **1963**, *39*, 1397–1412. (b) Ammeter, J. H.; Bürgi, H. B.; Thibeault, J.; Hoffmann, R. *J. Am. Chem. Soc.* **1978**, *100*, 3686–3692.

(30) Whangbo, M.-H.; Hoffmann, R. *J. Am. Chem. Soc.* **1978**, *100*, 6093–6098. Whangbo, M.-H.; Hoffmann, R.; Woodward, R. B. *Proc. R. Soc. London* **1979**, *A366*, 23–46.

**Table 6.** Atomic Parameters for  $(\text{NH}_2\text{Me}_2)_{0.5}[\text{Ni}(\text{dmit})_2]$  (4)

atom	$x/a$	$y/b$	$z/c$	$B_{\text{eq}}, \text{\AA}^2$
Ni	0.19776(5)	0.44988(2)	0.18274(6)	1.933(8)
S(1)	0.1795(1)	0.38289(5)	-0.1186(1)	2.29(2)
S(2)	0.0312(1)	0.20764(5)	-0.2940(1)	2.70(2)
S(3)	-0.1402(1)	0.04137(6)	-0.2716(2)	3.70(2)
S(4)	-0.0605(1)	0.17247(5)	0.0906(1)	2.73(2)
S(5)	0.0741(1)	0.34593(5)	0.2975(1)	2.49(2)
S(6)	0.3182(1)	0.55343(5)	0.0652(1)	2.41(2)
S(7)	0.4751(1)	0.72316(5)	0.2742(1)	2.63(2)
S(8)	0.5737(1)	0.85350(6)	0.6319(2)	3.72(2)
S(9)	0.3953(1)	0.68944(5)	0.6677(1)	2.65(2)
S(10)	0.2301(1)	0.51668(5)	0.4888(1)	2.51(2)
C(1)	0.0797(4)	0.2888(2)	-0.0931(5)	2.05(6)
C(2)	-0.0605(4)	0.1361(2)	-0.1621(5)	2.49(7)
C(3)	0.0355(4)	0.2727(2)	0.0878(5)	2.04(6)
C(4)	0.3704(4)	0.6258(2)	0.2770(5)	2.06(6)
C(5)	0.4841(4)	0.7598(2)	0.5303(5)	2.38(7)
C(6)	0.3327(4)	0.6093(2)	0.4644(5)	2.07(6)
N <sup>b</sup>	0.5594(8)	0.0243(4)	0.022(1)	4.5(2)
C(11) <sup>b</sup>	0.596(1)	-0.0511(5)	0.162(1)	4.3(2)
C(12) <sup>b</sup>	0.371(1)	0.0209(4)	-0.143(1)	3.6(2)

<sup>a</sup>  $B_{\text{eq}} = (4/3)\sum_i\sum_j\beta_{ij}a_j$ . <sup>b</sup> Structure occupation factor 0.5.

$(\text{NH}_2\text{Me}_2)_2[\text{M}(\text{dmit})_2]$  complexes can be also obtained using method *E*.

The very high solubility of the  $(\text{NH}_3\text{Me})_2[\text{M}(\text{dmit})_2]$  complexes prevented them from being easily isolated when using method *E*. For obtaining these complexes, we had to design and use method *I* (Scheme 3), which involves the preparation and isolation of the rather unstable  $\text{dmitNa}_2$  salt as starting material, and the recrystallization of  $(\text{NH}_3\text{Me})_2[\text{M}(\text{dmit})_2]$  in acetonitrile by ether addition. Method *I* can be used as well for the preparation of the  $(\text{NH}_2\text{Me}_2)_2[\text{M}(\text{dmit})_2]$  complexes.

The  $(\text{NH}_y\text{Me}_{4-y})[\text{M}(\text{dmit})_2]$  monovalent complexes with  $y = 1, 2$ , and 3 and  $\text{M} = \text{Ni}, \text{Pd}$ , and  $\text{Pt}$  were obtained from the corresponding divalent  $(\text{NH}_y\text{Me}_{4-y})_2[\text{M}(\text{dmit})_2]$  salts by oxidation with  $\text{I}_2/\text{NaI}$  or by air oxidation in the presence of acetic acid.

Because of their very high solubility, the  $(\text{NH}_4)_2[\text{M}(\text{dmit})_2]$  complexes could not be isolated as solid phases, even when using method *I*. However  $(\text{NH}_4)[\text{M}(\text{dmit})_2]$  complexes could be obtained directly, with extremely low yields, by  $\text{I}_2/\text{NaI}$  oxidation of an acetone solution of  $(\text{NH}_4)_2[\text{M}(\text{dmit})_2]$ .

The electrochemical data for all studied  $(\text{NH}_y\text{Me}_{4-y})[\text{M}(\text{dmit})_2]$  complexes are given in the supplementary material (Table S10). The voltammogram of  $(\text{NHMe}_3)[\text{Ni}(\text{dmit})_2]$  consists of two waves (Figure 5a). The first one at  $\approx -0.2$  V vs  $\text{Ag}/\text{AgCl}$ , is reversible and corresponds to the  $[\text{Ni}(\text{dmit})_2]^{2-}/[\text{Ni}(\text{dmit})_2]^-$  redox couple. The second one, quasireversible, shows features (sharp increase in the intensity of the anodic peak followed by a smooth decrease, high intensity of the backward redissolution peak) characteristic<sup>31</sup> of a modification of the anode due to the buildup of a  $(\text{NHMe}_3)_x$ - $[\text{Ni}(\text{dmit})_2]$  conductive species. In the case of the  $(\text{NHMe}_3)$ - $[\text{Pd}(\text{dmit})_2]$  analog (Figure 5b) both waves merge; however, when acetonitrile is substituted for acetone as solvent, these waves can be separated. The merging of these waves is intermediate in the case of the  $(\text{NHMe}_3)[\text{Pt}(\text{dmit})_2]$  analog (Figure 5c). The mechanism of formation of the non-integral oxidation state  $(\text{NMe}_4)_{0.5}[\text{Ni}(\text{dmit})_2]$  and  $(\text{NHMe}_3)_{0.5}[\text{Ni}(\text{dmit})_2]$  conductive species has been cleared up by use of fast voltage-scan cyclic voltammetry on ultramicroelectrodes.<sup>16</sup> This formation proceeds through a one-electron transfer ( $[\text{Ni}(\text{dmit})_2]^-/[\text{Ni}(\text{dmit})_2]^{0}$ ) combined with chemical reaction between  $[\text{Ni}(\text{dmit})_2]^-$  and the electrogenerated  $[\text{Ni}(\text{dmit})_2]^{0}$  species.

These preliminary electrochemical studies indicate that most of the  $(\text{NH}_y\text{Me}_{4-y})[\text{M}(\text{dmit})_2]$  complexes may be used as a source of possibly conducting  $(\text{NH}_y\text{Me}_{4-y})_x[\text{M}(\text{dmit})_2]$  phases. In fact, in most cases, compounds (mostly microcrystalline powders) exhibiting good conductivities (*vide infra*, Table 15) have been

**Table 7.** Atomic Parameters for  $(\text{NH}_3\text{Me})_2[\text{Ni}(\text{dmit})_2]_2 \cdot 2\text{MeCN}$  (5)

atom	$x/a$	$y/b$	$z/c$	$B_{\text{eq}}, \text{\AA}^2$
Ni(1)	$1/2$	$1/2$	$1/2$	2.18(3)
S(11)	0.4864(1)	0.5582(1)	0.7854(3)	2.85(5)
S(12)	0.4777(2)	0.7124(1)	0.8932(4)	3.22(5)
S(13)	0.4821(2)	0.8585(1)	0.7921(5)	4.45(7)
S(14)	0.4991(2)	0.7427(1)	0.4776(4)	3.19(5)
S(15)	0.5055(1)	0.5922(1)	0.3363(3)	2.71(5)
C(11)	0.4874(5)	0.6409(5)	0.720(1)	2.6(2)
C(12)	0.4850(5)	0.7766(5)	0.723(1)	3.0(2)
C(13)	0.4954(5)	0.6577(5)	0.520(1)	2.3(2)
Ni(2)	0.09947(7)	0.53506(7)	0.7172(2)	2.42(2)
S(21)	0.0935(1)	0.4430(1)	0.8813(3)	2.95(5)
S(22)	0.1041(2)	0.2902(1)	0.7403(4)	3.32(6)
S(23)	0.1246(2)	0.1750(2)	0.4195(5)	5.35(8)
S(24)	0.1229(2)	0.3226(1)	0.3234(4)	3.21(6)
S(25)	0.1147(1)	0.4759(1)	0.4332(3)	2.89(5)
S(26)	0.0798(1)	0.5967(1)	0.9993(3)	2.72(5)
S(27)	0.0704(2)	0.7527(1)	1.0968(4)	3.64(6)
S(28)	0.0719(2)	0.8991(2)	0.9907(6)	5.90(8)
S(29)	0.0943(2)	0.7798(1)	0.6824(4)	3.68(6)
S(30)	0.1074(2)	0.6260(1)	0.5498(3)	3.10(5)
C(21)	0.1038(5)	0.3791(5)	0.699(1)	2.7(2)
C(22)	0.1176(6)	0.2573(5)	0.492(2)	3.2(2)
C(23)	0.1128(5)	0.3938(5)	0.496(1)	2.4(2)
C(24)	0.0826(5)	0.6800(5)	0.927(1)	2.5(2)
C(25)	0.0788(6)	0.8153(6)	0.924(2)	4.0(3)
C(26)	0.0944(5)	0.6929(5)	0.732(1)	2.7(2)
Ni(3)	0.30005(7)	0.42957(6)	0.0192(2)	2.27(2)
S(31)	0.2865(1)	0.4901(1)	0.3025(3)	2.89(5)
S(32)	0.2822(2)	0.6438(1)	0.4015(3)	3.21(5)
S(33)	0.2873(2)	0.7881(2)	0.2856(5)	5.13(8)
S(34)	0.2999(2)	0.6714(1)	-0.0200(4)	3.17(5)
S(35)	0.3050(1)	0.5207(1)	-0.1520(3)	2.79(5)
S(36)	0.2921(1)	0.3394(1)	0.1893(3)	2.85(5)
S(37)	0.3057(2)	0.1849(1)	0.0592(4)	3.20(5)
S(38)	0.3352(2)	0.0621(2)	-0.2431(5)	4.75(7)
S(39)	0.3339(2)	0.2096(1)	-0.3533(4)	3.28(6)
S(40)	0.3212(1)	0.3667(1)	-0.2592(3)	2.63(5)
C(31)	0.2891(5)	0.5716(5)	0.231(1)	2.7(2)
C(32)	0.2900(6)	0.7048(5)	0.229(2)	3.2(2)
C(33)	0.2978(5)	0.5860(5)	0.030(1)	2.6(2)
C(34)	0.3057(5)	0.2728(5)	0.008(1)	2.6(2)
C(35)	0.3254(6)	0.1474(5)	-0.184(1)	3.2(2)
C(36)	0.3192(5)	0.2841(5)	-0.189(1)	2.5(2)
N(3)	0.3086(8)	0.9576(7)	0.268(2)	7.6(3) <sup>b</sup>
C(51)	0.3694(8)	0.9624(7)	0.277(2)	5.4(3) <sup>b</sup>
C(52)	0.4415(8)	0.9725(8)	0.287(2)	6.0(3) <sup>b</sup>
N(1) <sup>c</sup>	0.1298(8)	0.0781(8)	0.915(2)	4.83(4) <sup>b</sup>
C(41) <sup>c</sup>	0.1798(9)	0.0036(8)	0.858(2)	3.50(4) <sup>b</sup>
N(2) <sup>c</sup>	0.2622(7)	0.8792(7)	0.754(2)	4.05(3) <sup>b</sup>
C(42) <sup>c</sup>	0.2110(9)	0.9539(9)	0.802(3)	4.11(4) <sup>b</sup>

<sup>a</sup>  $B_{\text{eq}} = (4/3)\sum_i\sum_j\beta_{ij}a_j$ . <sup>b</sup> Atom refined isotropically. <sup>c</sup> The  $(\text{NH}_3\text{Me})^+$  cation is statistically distributed over two sets of positions. The structure occupation factor (50%) was estimated on the basis of the similarity of isotropic temperature factors.

obtained by galvanostatic oxidation of a solution of the appropriate  $(\text{NH}_y\text{Me}_{4-y})[\text{M}(\text{dmit})_2]$  complex, or of a solution of  $(\text{NBu}_4)[\text{M}(\text{dmit})_2]$  in the presence of a very large excess of  $(\text{NH}_4)\text{Cl}$  in the case of the  $(\text{NH}_4)_x[\text{M}(\text{dmit})_2]$  compounds. Crystals of size and quality suitable for further studies have been obtained in seven cases (Table 1).

$(\text{NMe}_4)_{0.5}[\text{Ni}(\text{dmit})_2]$  (1). This compound has been reported as superconducting under pressure,<sup>9</sup> but this behavior was observed for just one crystal of this phase.<sup>32</sup> We have prepared samples of this compound, and the X-ray study of the platelet-like single crystals confirms that the same phase has been obtained [monoclinic, space group  $\text{C}2/c$ ,  $a = 13.856(3)$  Å,  $b = 6.533(3)$  Å,  $c = 36.083(12)$  Å,  $\beta = 93.78(2)^\circ$ ,  $V = 3259(1)$  Å<sup>3</sup>; to be compared with<sup>9</sup> monoclinic, space group  $\text{C}2/c$ ,  $a = 13.856(4)$  Å,  $b = 6.498(2)$  Å,  $c = 36.053(11)$  Å,  $\beta = 93.83(3)^\circ$ ,  $V = 3229(1)$  Å<sup>3</sup>].

(31) Valade, L.; Cassoux, P.; Gleizes, A.; Interrante, L. V. *J. Phys. (Paris)* 1983, 44 (C3), 1183-1188.

(32) Kobayashi, A.; Kobayashi, H. Personal communication.

Table 8. Atomic Parameters for (NHMe<sub>3</sub>)<sub>2</sub>[Pt(dmit)<sub>2</sub>]<sub>3</sub>·MeCN (7)

atom	<i>x/a</i>	<i>y/b</i>	<i>z/c</i>	<i>B</i> <sub>eq</sub> <sup>a</sup> , Å <sup>2</sup>
Pt(1)	0.32897(4)	0.49229(3)	0.12735(7)	2.24(1)
S(11)	0.2046(2)	0.4112(2)	0.1537(6)	2.6(1)
S(12)	0.1518(2)	0.2521(2)	0.2537(6)	3.4(1)
S(13)	0.1811(3)	0.1143(3)	0.3845(8)	5.9(2)
S(14)	0.3149(2)	0.2442(2)	0.3054(6)	3.2(1)
S(15)	0.3867(2)	0.4018(2)	0.2072(6)	2.7(1)
S(16)	0.2685(2)	0.5776(2)	0.0204(6)	2.7(1)
S(17)	0.3345(2)	0.7274(2)	-0.1125(6)	3.2(1)
S(18)	0.4652(3)	0.8569(2)	-0.1998(6)	4.0(1)
S(19)	0.4978(2)	0.7193(2)	-0.0736(6)	3.0(1)
S(20)	0.4504(2)	0.5672(3)	0.0669(6)	2.7(1)
C(11)	0.2271(9)	0.3337(8)	0.220(2)	2.9(4)
C(12)	0.214(1)	0.1976(9)	0.318(2)	3.6(4)
C(13)	0.3046(8)	0.3301(7)	0.240(2)	2.1(3)
C(14)	0.3475(8)	0.6462(8)	-0.030(2)	2.5(4)
C(15)	0.4344(8)	0.7733(8)	-0.130(2)	2.8(4)
C(16)	0.4258(8)	0.6434(8)	-0.010(2)	2.3(4)
Pt(2)	0.35988(3)	0.56842(3)	0.49534(8)	2.24(2)
S(21)	0.4191(2)	0.4832(2)	0.6062(6)	2.6(1)
S(22)	0.3519(2)	0.3346(2)	0.7467(6)	2.8(1)
S(23)	0.2184(3)	0.2071(2)	0.8334(6)	4.3(1)
S(24)	0.1891(2)	0.3424(2)	0.6941(6)	3.0(1)
S(25)	0.2379(2)	0.4925(2)	0.5512(6)	2.6(1)
S(26)	0.4848(2)	0.6496(2)	0.4696(6)	2.50(9)
S(27)	0.5382(2)	0.8112(2)	0.3831(6)	3.3(1)
S(28)	0.5132(3)	0.9568(3)	0.2968(8)	5.4(1)
S(29)	0.3757(2)	0.8207(2)	0.3368(6)	3.4(1)
S(30)	0.3027(2)	0.6606(2)	0.4184(6)	2.64(9)
C(21)	0.3363(9)	0.4144(7)	0.663(2)	2.0(3)
C(22)	0.2505(8)	0.2891(9)	0.762(2)	3.1(4)
C(23)	0.2626(9)	0.4183(8)	0.637(2)	3.0(4)
C(24)	0.4634(8)	0.7309(8)	0.412(2)	2.6(4)
C(25)	0.4781(9)	0.8687(8)	0.337(2)	3.3(4)
C(26)	0.3848(8)	0.7333(8)	0.391(2)	2.6(4)
Pt(3)	-0.01696(3)	0.46107(4)	0.30880(9)	2.44(1)
S(31)	0.1034(2)	0.5407(3)	0.2549(6)	3.0(1)
S(32)	0.1464(2)	0.6941(2)	0.1210(6)	3.2(1)
S(33)	0.1075(3)	0.8313(3)	0.0041(6)	4.4(1)
S(34)	-0.0182(3)	0.6975(2)	0.0825(6)	3.1(1)
S(35)	-0.0802(2)	0.5441(3)	0.2066(6)	2.9(1)
S(36)	-0.1407(2)	0.3799(2)	0.3375(6)	2.7(1)
S(37)	-0.1930(2)	0.2175(2)	0.4214(6)	3.2(1)
S(38)	-0.1666(3)	0.0719(3)	0.5000(7)	5.3(1)
S(39)	-0.0302(2)	0.2093(2)	0.4655(6)	3.4(1)
S(40)	0.0417(2)	0.3703(2)	0.3856(6)	2.8(1)
C(31)	0.0764(9)	0.6135(8)	0.174(2)	2.3(4)
C(32)	0.0809(8)	0.7456(8)	0.067(2)	2.6(4)
C(33)	-0.0038(8)	0.6159(8)	0.158(2)	2.3(4)
C(34)	-0.0399(9)	0.2960(8)	0.415(2)	2.7(4)
C(35)	-0.1312(9)	0.1609(8)	0.465(2)	3.1(4)
C(36)	-0.1176(8)	0.3000(8)	0.393(2)	2.3(4)
N(1)	0.2890(9)	0.9979(9)	1.011(3)	6.6(5)
C(41)	0.318(1)	0.938(1)	0.937(3)	5.7(6)
C(42)	0.308(1)	1.006(2)	1.205(3)	8.8(9)
C(43)	0.321(1)	1.071(1)	0.940(4)	8.3(8)
N(3)	0.128(1)	0.009(1)	0.920(3)	9.2(8)
C(51)	0.081(1)	0.031(1)	0.855(3)	6.1(6)
C(52)	0.018(1)	0.058(2)	0.761(4)	12.1(1)

$$^a B_{eq} = (4/3) \sum_i \sum_j \beta_{ij} a_j$$

As previously reported,<sup>9</sup> the ambient-pressure room-temperature single-crystal conductivity is 55 S·cm<sup>-1</sup>, and a metal-like temperature-dependent behavior is observed down to 90 K. However, no hysteresis is observed in our measurements: the conductivity values determined when decreasing or increasing the temperature are identical. Moreover, conductivity measurements carried out on our samples at 10 kbar and from 300 to 4 K did not show any superconducting transition similar to that previously reported.<sup>9</sup> These apparent contradictions show how sensitive to the crystal quality the electrical properties of such compounds can be.

(NHMe<sub>3</sub>)<sub>0.5</sub>[Ni(dmit)<sub>2</sub>] (2). Hexagonal plateletlike crystals of this phase have been characterized by X-ray diffraction methods

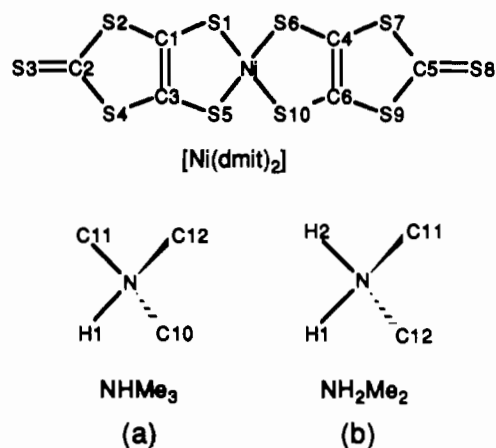


Figure 2. Atomic numbering scheme for (a) (NHMe<sub>3</sub>)<sub>0.5</sub>[Ni(dmit)<sub>2</sub>] (2) and (b) (NH<sub>2</sub>Me<sub>2</sub>)<sub>0.5</sub>[Ni(dmit)<sub>2</sub>] (4).

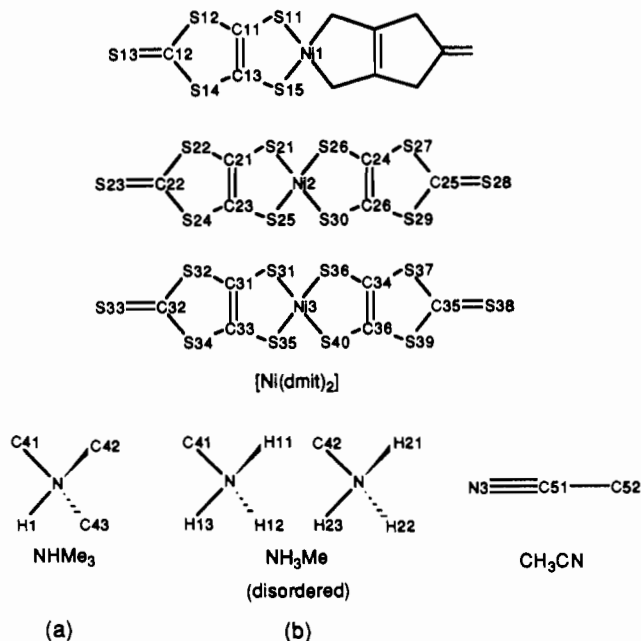


Figure 3. Atomic numbering scheme for (a) (NHMe<sub>3</sub>)<sub>2</sub>[Ni(dmit)<sub>2</sub>]<sub>5</sub>·2MeCN (3) and (b) (NH<sub>3</sub>Me)<sub>2</sub>[Ni(dmit)<sub>2</sub>]<sub>5</sub>·2MeCN (5).

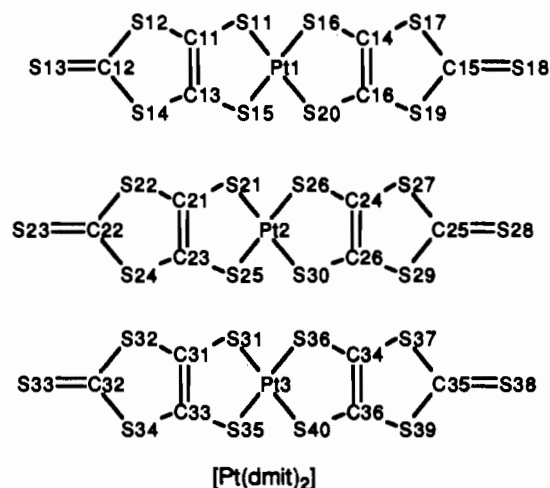


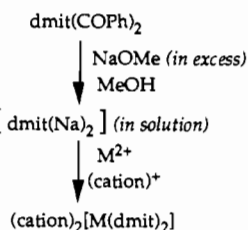
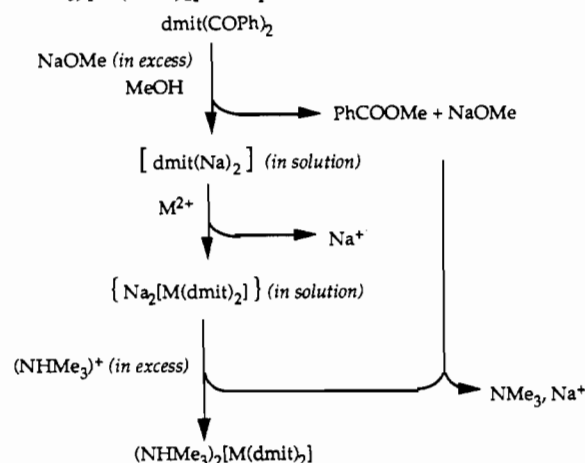
Figure 4. Atomic numbering scheme for the [Pt(dmit)<sub>2</sub>] entities of (NHMe<sub>3</sub>)<sub>2</sub>[Pt(dmit)<sub>2</sub>]<sub>3</sub>·MeCN (7). Atomic numbering scheme for (NHMe<sub>3</sub>)<sup>+</sup> and MeCN as in Figure 3.

(Figure 2; Tables 2 and 4). Bond lengths and angles are listed in Table 10. The Ni(dmit)<sub>2</sub> units are practically planar (deviations of the atoms to their least-squares plane less than 0.01 Å). The N atom (0.927; 0.0146; 0.435) of the (NHMe<sub>3</sub>)<sup>+</sup> cation is close to the center of symmetry (1; 0; 1/2); thus these cations are

**Table 9.** Exponents and Parameters Used in the Calculations

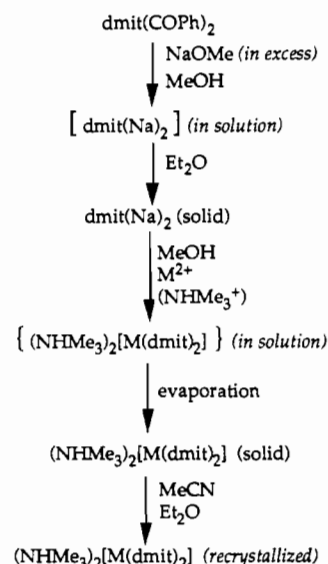
atom	orbital	$H_{ii}$ , eV	$\zeta_1$	$c_1^a$	$\zeta_2$	$c_2^a$
Ni <sup>38</sup>	4s	-9.70	2.10			
	4p	-5.15	2.10			
	3d	-13.49	5.75	0.5798	2.30	0.5782
Pt <sup>30a</sup>	6s	-9.08	2.554			
	6p	-5.47	2.554			
	5d	-12.59	6.013	0.6334	2.696	0.5513
S <sup>38</sup>	3s	-20.00	1.817			
	3p	-13.30	1.817			
C <sup>38</sup>	2s	-21.40	1.625			
	2p	-11.40	1.625			

<sup>a</sup> Contraction coefficients used in the double- $\zeta$  expansion.

**Scheme 1.** Standard Method for the Preparation of the (cation)<sub>2</sub>[M(dmit)<sub>2</sub>] Complexes**Scheme 2.** Method of Excess (E) for the Preparation of the (NHMe<sub>3</sub>)<sub>2</sub>[M(dmit)<sub>2</sub>] Complexes

disordered and statistically (50%–50%) occupy two groups of general positions related through this center of symmetry. Hence, the  $x = 0.5$ , or 1:2 stoichiometry<sup>22</sup> of (NHMe<sub>3</sub>)<sub>0.5</sub>[Ni(dmit)<sub>2</sub>] is ascertained. The content of the unit cell is shown in Figure 6. The structure consists of Ni(dmit)<sub>2</sub> layers separated by sheets of (NHMe<sub>3</sub>)<sup>+</sup> cations. The Ni(dmit)<sub>2</sub> units are stacked along the [100] direction and weakly dimerized (Figure 7). Within a stack, the distances between the mean planes of two Ni(dmit)<sub>2</sub> units are 3.51 and 3.60 Å, alternately. As in most [M(dmit)<sub>2</sub>]-based systems,<sup>3</sup> a number of intermolecular sulfur...sulfur distances shorter than the sum of the van der Waals radii (3.7 Å) are observed between Ni(dmit)<sub>2</sub> molecules belonging to the same stack (intrastack contacts) or to adjacent stacks (interstack contacts) (supplementary material, Table S11).

The ambient pressure room-temperature conductivity is quite high, 140 S·cm<sup>-1</sup> (even higher than that of superconducting (NMe<sub>4</sub>)<sub>0.5</sub>[Ni(dmit)<sub>2</sub>], *vide supra*), and the conductivity remains almost constant down to 220 K. Below this temperature, the compound becomes insulating (Figure 8a), and a hysteresis is observed in the conductivity behavior when decreasing and increasing again the temperature (supplementary material, Figure SF1).<sup>20</sup> This is probably due to nonannealed cracks formation during the first cooling step, but subsequent thermal cycling does not induce any further shift in the temperature dependence of the conductivity. Moreover, a 2% increase in the conductivity is observed after 2 h of annealing at 328 K.

**Scheme 3.** Method of Isolation (I) for the Preparation of the (NHMe<sub>3</sub>)<sub>2</sub>[M(dmit)<sub>2</sub>] Complexes

Conductivity measurements at 3.5 kbar did not show any superconducting transition, but, contrary to what was observed in (NMe<sub>4</sub>)<sub>0.5</sub>[Ni(dmit)<sub>2</sub>],<sup>9</sup> the conductivity decreases with increasing pressure (Figure 8). As shown in Figure 8, the conductivity of this compound, determined by AC measurements, seems to depend on the current. Careful DC measurements at low temperature confirm this nonlinear dependence of the conductivity on the current intensity. This is observed by plotting the differential resistance  $dV/dI$  as a function of the current. Typical bell-shaped curves are observed and the lower the temperature, the more pronounced the nonohmic behavior: at 4.6 K for example,  $dV/dI$  drops by 1 order of magnitude when the current increases from zero to only 4 μA (Figure 9). Such nonlinear behavior has also been observed in several compounds exhibiting CDW transition.<sup>33</sup> However, it has been also observed in the (NMe<sub>4</sub>)<sub>0.5</sub>[Ni(dmit)<sub>2</sub>] phase for which no sign of CDW has been detected.<sup>34,35</sup> No activation energy can be derived from the data shown in Figure 8; in addition, the temperature dependence of the conductivity cannot be accounted for by any variable range hopping model, involving or not involving Coulombian correlations.<sup>36,37</sup>

As far as artifacts resulting from Joule heating or from the existence of "microcracks" in the crystal can be excluded, a possible explanation of the conductivity behavior of (NHMe<sub>3</sub>)<sub>0.5</sub>[Ni(dmit)<sub>2</sub>] (hysteresis, increase of conductivity upon annealing, nonohmic character, decrease of conductivity with increasing pressure), could then involve an electron localization induced by disorder or defects. In this compound, in addition to the disorder possibly arising from the rotation degrees of freedom of the hydrogens of methyl groups around the N–C axes, another disorder results from the two positions that the (NHMe<sub>3</sub>)<sup>+</sup> cations may occupy (*vide supra*). The localization of the carriers may be due to the fluctuating potential along the stacks of Ni(dmit)<sub>2</sub> and the increase of conductivity with increasing current can be related to the weakening influence of these potential fluctuations compared to that of the translation energy.

An alternative interpretation may be also proposed by comparing the electronic band structures of **1** and **2**, as discussed in the following section.

(33) Monceau, P.; Richard, J. *Phys. Rev. B* **1988**, *37*, 7982–7985.

(34) Kobayashi, A.; Kim, H.; Sasaki, Y.; Moriyama, S.; Nishio, Y.; Kajita, K.; Sasaki, W.; Kato, R.; Kobayashi, H. *Synth. Met.* **1988**, *27B*, 339–346.

(35) Ravy, S. Personal communication.

(36) Mott, N. F. *J. Non-Cryst. Solids* **1968**, *1*, 1–17.

(37) Audouard, A.; Kazoun, A.; Cherradi, N.; Marchal, G.; Gerl, M. *Philos. Mag. B* **1989**, *59*, 207–220.

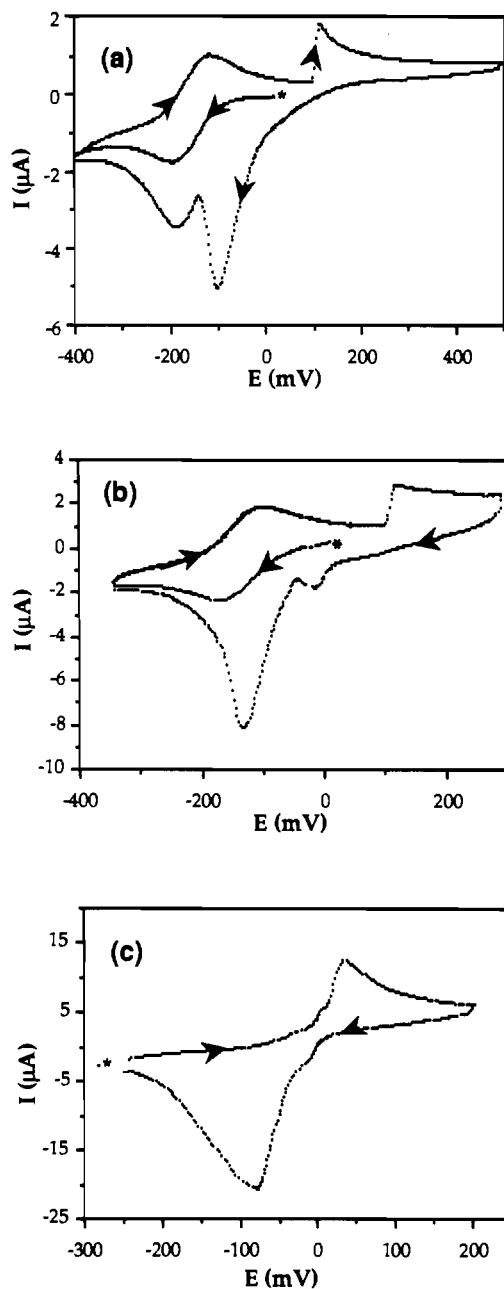


**Figure 5.** Cyclic voltammetry of (NHMe<sub>3</sub>)M(dmit)<sub>2</sub>, 10<sup>-3</sup> mol/L, in MeCN containing (NHMe<sub>3</sub>)BF<sub>4</sub>, 0.1 mol/L. Key: \* starting potential; potential scan rate 0.1 V/s; potential in mV vs Ag/AgCl; (a) M = Ni; (b) M = Pd; (c) M = Pt.

**Electronic Band Structures of (NMe<sub>4</sub>)<sub>0.5</sub>[Ni(dmit)<sub>2</sub>] (1) and (NHMe<sub>3</sub>)<sub>0.5</sub>[Ni(dmit)<sub>2</sub>] (2).** The minute modification consisting of substituting a methyl group in 1 for a hydrogen atom in 2 results in both cases in similar overall arrangement of layers of Ni(dmit)<sub>2</sub> stacked molecules with similar alternating stacking distances, separated by sheets of cations (see Figures 6 and 7 and ref 9). However, whereas 1 is monoclinic with space group C2/c, 2 is triclinic with space group P1̄. Thus, two Ni(dmit)<sub>2</sub> stacking directions related by symmetry, [110] and [1̄10], are observed in 1, but only one, [100], in (2). The energy dispersion curves calculated for the Ni(dmit)<sub>2</sub> layers of both compounds are very similar (Figure 10).

As is often the case for compounds where the Ni(dmit)<sub>2</sub> entities are weakly dimerized along the stacking direction, the two LUMO bands lie above the two HOMO bands.<sup>8,38</sup> The calculated Fermi

**Table 10.** Bond Lengths (Å) and Angles (deg) for (NHMe<sub>3</sub>)<sub>0.5</sub>[Ni(dmit)<sub>2</sub>] (2)

Ni-S(1)	2.167(1)	S(7)-C(5)	1.691(5)
Ni-S(2)	2.160(1)	S(8)-C(4)	1.745(5)
Ni-S(6)	2.168(1)	S(8)-C(6)	1.734(5)
Ni-S(7)	2.153(1)	S(9)-C(5)	1.741(5)
S(1)-C(1)	1.715(5)	S(9)-C(6)	1.726(6)
S(2)-C(2)	1.705(5)	S(10)-C(6)	1.646(5)
S(3)-C(1)	1.743(5)	C(1)-C(2)	1.368(7)
S(3)-C(3)	1.731(6)	C(4)-C(5)	1.377(7)
S(4)-C(2)	1.736(5)	N <sup>a</sup> -C(13) <sup>a</sup>	1.42(2)
S(4)-C(3)	1.726(6)	N <sup>a</sup> -C(15) <sup>a</sup>	1.51(2)
S(5)-C(3)	1.653(5)	N <sup>a</sup> -C(16) <sup>a</sup>	1.46(2)
S(6)-C(4)	1.698(5)		
S(1)-Ni-S(2)	93.44(5)	S(3)-C(3)-S(4)	113.3(3)
S(1)-Ni-S(6)	88.39(5)	S(3)-C(3)-S(5)	123.6(4)
S(1)-Ni-S(7)	178.06(6)	S(4)-C(3)-S(5)	123.0(4)
S(2)-Ni-S(6)	178.06(6)	S(6)-C(4)-S(8)	123.3(3)
S(2)-Ni-S(7)	85.16(5)	S(6)-C(4)-C(5)	121.3(4)
S(6)-Ni-S(7)	93.03(5)	S(8)-C(4)-C(5)	115.4(4)
C(1)-S(3)-C(3)	97.3(2)	S(7)-C(5)-S(9)	122.6(3)
C(2)-S(4)-C(3)	97.5(3)	S(7)-C(5)-C(4)	121.2(4)
C(4)-S(8)-C(6)	97.4(2)	S(9)-C(5)-C(4)	116.2(4)
C(5)-S(9)-C(6)	97.4(2)	S(8)-C(6)-S(9)	113.6(3)
S(1)-C(1)-S(3)	123.0(3)	S(8)-C(6)-S(10)	124.3(3)
S(1)-C(1)-C(2)	121.3(4)	S(9)-C(6)-S(10)	122.1(3)
S(3)-C(1)-C(2)	115.7(4)	C(10) <sup>a</sup> -N <sup>a</sup> -C(11) <sup>a</sup>	113(2)
S(2)-C(2)-S(4)	122.4(3)	C(10) <sup>a</sup> -N <sup>a</sup> -C(12) <sup>a</sup>	108(2)
S(2)-C(2)-C(1)	121.5(4)	C(11) <sup>a</sup> -N <sup>a</sup> -C(12) <sup>a</sup>	110(2)
S(4)-C(2)-C(1)	116.1(4)		

<sup>a</sup> Structure occupation factor 0.5.

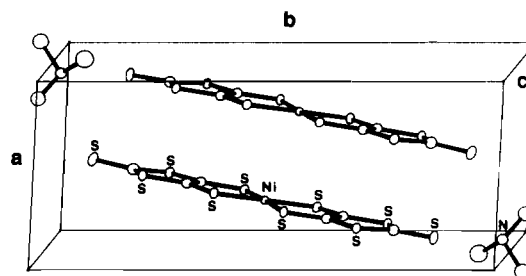


**Figure 6.** Unit cell of (NHMe<sub>3</sub>)<sub>0.5</sub>[Ni(dmit)<sub>2</sub>] (2). The (NHMe<sub>3</sub>)<sup>+</sup> cations are disordered; for clarity only one of the two groups of positions statistically occupied is drawn.

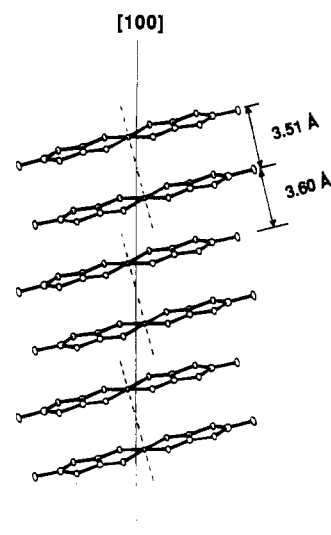


**Figure 7.** Stacking mode in (NHMe<sub>3</sub>)<sub>0.5</sub>[Ni(dmit)<sub>2</sub>] (2).

surfaces for a Ni(dmit)<sub>2</sub> layer of 1 and 2 are shown in parts a and b of Figure 11, respectively. The two Fermi surfaces are almost identical. However, since 1 contains two Ni(dmit)<sub>2</sub> layers per unit cell, the Fermi surface of 1 actually is the superposition of two identical Fermi surfaces corresponding to the two symmetry related layers of Ni(dmit)<sub>2</sub> units stacked along [110] and [1̄10],

(38) Canadell, E.; Rachidi, E. I.; Ravy, S.; Pouget, J.-P.; Brossard, L.; Legros, J.-P. *J. Phys. (Paris)* **1989**, *50*, 2967-2981; Ravy, S.; Canadell, E.; Pouget, J.-P.; Cassoux, P.; Underhill, A. E. *Synth. Met.* **1991**, *41-43*, 2191-2194.

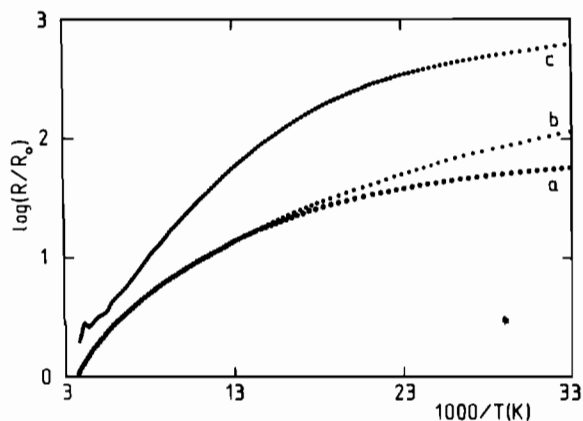


**Figure 8.** Logarithmic variation of the resistance  $R$  of  $(\text{NHMe}_3)_{0.5}[\text{Ni}(\text{dmit})_2]$  (**2**) relative to  $R_0$  (at 300 K) vs  $T^{-1}$ : (a) ambient pressure,  $I = 100 \mu\text{A}$ ; (b) ambient pressure,  $I = 1 \mu\text{A}$ ; (c) 3.5 kbar pressure,  $I = 1.5 \mu\text{A}$ .

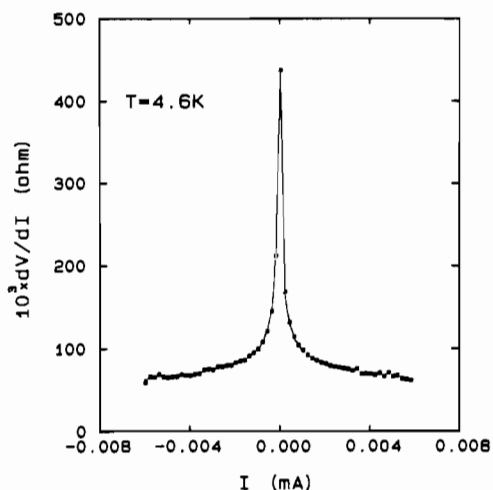


**Figure 9.** Differential resistance vs current at  $T = 4.6 \text{ K}$  for  $(\text{NHMe}_3)_{0.5}[\text{Ni}(\text{dmit})_2]$  (**2**).

respectively (Figure 11c). The Fermi surfaces of Figure 11a and b are quite one-dimensional and perpendicular to the direction of the stacks. Hence, one can speculate that the metal-to-insulator transitions in **1** and **2** originate from a CDW instability. However, because of the presence of two  $\text{Ni}(\text{dmit})_2$  layers in **1**, a CDW condensation in this salt can only occur if the nesting vectors of the two Fermi surfaces are close enough so that the same distortion can destroy the two Fermi surfaces simultaneously. Such a situation has been proven to occur in  $\text{Cs}[\text{Pd}(\text{dmit})_2]_2$ .<sup>39</sup> In view of the quite different directions of stacking, a common nesting vector would only occur if the Fermi surfaces of the  $\text{Ni}(\text{dmit})_2$  layers were purely one-dimensional (i.e., the warping was negligible). Because of the warping of the Fermi surfaces in Figure 11c, a CDW condensation can hardly account for the metal-to-insulator transition observed in **1**. On the other hand, the Fermi surface of **2** (Figure 11b) is quite well nested, practically one-dimensional, and perpendicular to the unique [100] stacking direction. Therefore, in spite of the fact that up to now no clear indication of CDW condensation has been observed, the existence of a CDW in **2** cannot be ruled out until diffuse X-ray scattering measurements are carried out.

$(\text{NHMe}_3)_2[\text{Ni}(\text{dmit})_2]_5 \cdot 2\text{MeCN}$  (**3**). In several electrocrystallization experiments, in addition to the hexagonal platelets which have been characterized as  $(\text{NHMe}_3)_{0.5}[\text{Ni}(\text{dmit})_2]$  (**2**), long and thin, shiny, needle-like crystals have been simultaneously collected and characterized by X-ray diffraction methods as the

(39) Underhill, A. E.; Clark, R. A.; Marsden, I.; Allan, M.; Friend, R. H.; Tajima, H.; Naito, T.; Tamura, M.; Kuroda, H.; Kobayashi, A.; Kobayashi, H.; Canadell, E.; Ravy, S.; Pouget, J. P. *J. Phys.: Condens. Matter* **1991**, *3*, 933–954.

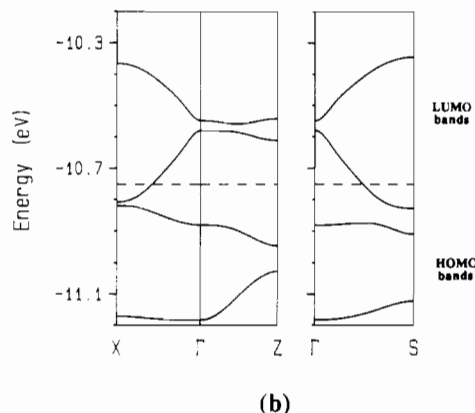
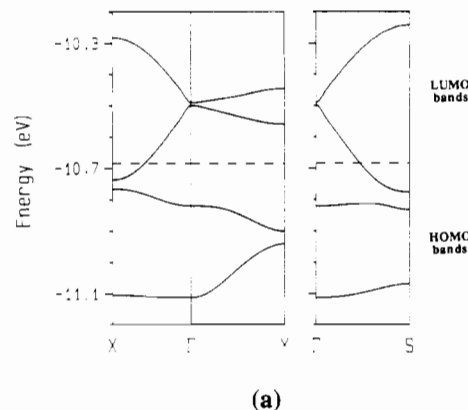


**Figure 10.** Band structure for the  $\text{Ni}(\text{dmit})_2$  slabs in: (a)  $(\text{NHMe}_3)_{0.5}[\text{Ni}(\text{dmit})_2]$  (**1**);  $\Gamma$ ,  $X$ ,  $Y$ , and  $S$  refer to the wave vectors  $(0, 0)$ ,  $(a_0^*/2, 0)$ ,  $(0, b_0^*/2)$ , and  $(-a_0^*/2, b_0^*/2)$ , respectively, with  $a_0 = (a + b)/2$  and  $b_0 = -b$ .<sup>38</sup> (b)  $(\text{NHMe}_3)_{0.5}[\text{Ni}(\text{dmit})_2]$  (**2**);  $\Gamma$ ,  $X$ ,  $Z$  and  $S$  refer to the wave vectors  $(0, 0)$ ,  $(a^*/2, 0)$ ,  $(0, c^*/2)$ , and  $(-a^*/2, c^*/2)$ , respectively. The dashed lines refer to the Fermi level.

$(\text{NHMe}_3)_2[\text{Ni}(\text{dmit})_2]_5 \cdot 2\text{MeCN}$  phase (Figure 3; Tables 2 and 5). Bond lengths and angles are listed in Table 11. The asymmetric unit contains three crystallographically independent nickel atoms, one of them lying on a center of symmetry. All three  $\text{Ni}(\text{dmit})_2$  units are practically planar (deviations of the atoms to their respective least-squares plane less than  $0.03 \text{ \AA}$ ). The content of the unit cell is shown in Figure 12. The structure consists of  $\text{Ni}(\text{dmit})_2$  layers parallel to the (010) plane separated by sheets of  $(\text{NHMe}_3)^+$  cations and solvent molecules along the [010] direction. The  $\text{Ni}(\text{dmit})_2$  units are stacked along the [102] direction (Figure 13). The stacking mode can be described as the repetition of a centrosymmetric pattern built of two weak dimers and one single molecule. The intradimer distance is  $3.55 \text{ \AA}$ , the interdimer distance is  $3.58 \text{ \AA}$ , and the distance between a dimer and the single  $\text{Ni}(\text{dmit})_2$  molecule is  $3.53 \text{ \AA}$ . Short ( $< 3.7 \text{ \AA}$ ) intermolecular intrastack and interstack sulfur...sulfur contacts are observed between neighboring  $\text{Ni}(\text{dmit})_2$  molecules (supplementary material, Table S12).

Single-crystal, temperature-dependent conductivity measurements along the needle axis show a semiconducting behavior (room-temperature conductivity  $\sigma_{\text{RT}} = 0.2 \text{ S}\cdot\text{cm}^{-1}$ ; activation energy  $E_a = 0.23 \text{ eV}$ ).

Because of the 2:5 stoichiometry, two electrons are transferred to a group of five  $\text{Ni}(\text{dmit})_2$  units. This raises the question of what is the oxidation state of the three symmetry inequivalent  $\text{Ni}(\text{dmit})_2$  units in **3**. Analysis of the internal structure of the acceptor layers shows that there are 10 different types of  $\text{Ni}(\text{dmit})_2 \cdots \text{Ni}(\text{dmit})_2$  interactions associated with sulfur...sulfur distances smaller than  $3.7 \text{ \AA}$  (supplementary material, Table S12). In order to quantify the strength of these interactions we have calculated their  $\beta_{ij}$  ( $i, j = \text{LUMO}, \text{LUMO}$ ) interaction energies.<sup>40</sup> These interaction energies reflect the strength of interaction between a pair of molecular orbitals in adjacent sites of the crystal and give important clues relating the electronic and

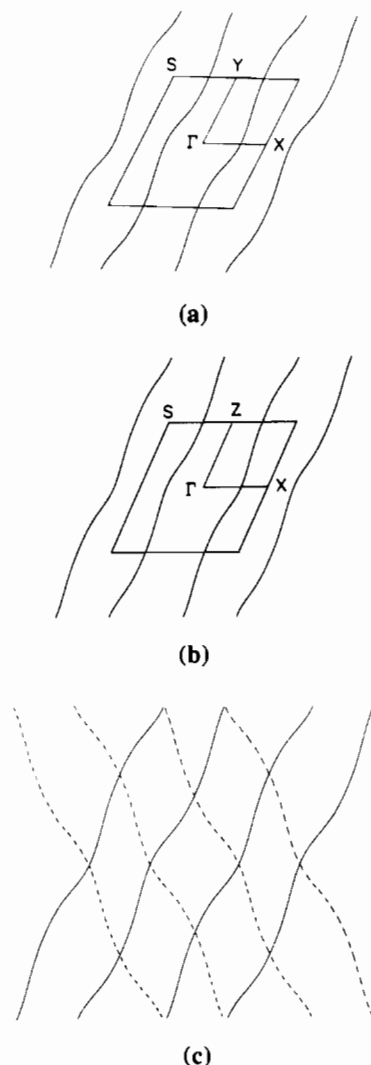


Figure 11. (a, b) Fermi surface of a Ni(dmit)<sub>2</sub> layer: (a) (NMe<sub>4</sub>)<sub>0.5</sub>[Ni(dmit)<sub>2</sub>] (1); (b) (NHMe<sub>3</sub>)<sub>0.5</sub>[Ni(dmit)<sub>2</sub>] (2). (c) Superposition of the Fermi surfaces of the two Ni(dmit)<sub>2</sub> layers of (NMe<sub>4</sub>)<sub>0.5</sub>[Ni(dmit)<sub>2</sub>] (1).

crystal structures of molecular conductors.<sup>40a</sup> Our calculations show that the intradimer interaction is relatively strong ( $\beta_{\text{LUMO-LUMO}} = 0.28$  eV) and of the same order of magnitude as the intradimer interaction in **1** and **2**. Consequently, every dimer will have a low-lying empty molecular orbital ( $\Psi^*_{\text{LUMO}}$ ) which is the bonding combination of the LUMOs of the two units of the dimer. This orbital is about 0.17 eV lower in energy than the LUMO of the single molecule inbetween the dimers. The interdimer interaction along the stacks is weaker ( $\beta_{\text{LUMO-LUMO}} = 0.05$  eV) and the interaction between the single molecule and the dimer is even weaker ( $\beta_{\text{LUMO-LUMO}} = 0.02$  eV). The seven different types of interstack interactions are all weak (i.e.,  $\beta_{\text{LUMO-LUMO}}$  values between 0.04 and 0.004 eV) even if some of them are associated with the shortest sulfur-sulfur intermolecular distances in the layer. These results suggest that the two transferred electrons will be housed one on each dimer and that the interactions between these electrons will be weak. Calculations for the Ni(dmit)<sub>2</sub> layer of **3** completely substantiate this analysis. Thus, we conclude that the Ni(dmit)<sub>2</sub> layers of **3** can be described as a series of weakly interacting single electrons located at the dimers, which explains the activated conductivity behavior. From

Table 11. Bond Lengths (Å) and Angles (deg) for (NHMe<sub>3</sub>)<sub>2</sub>[Ni(dmit)<sub>2</sub>]<sub>2</sub>·2MeCN (**3**)

Ni(1)-S(11)	2.1441(7)	S(12)-C(12)	1.724(2)
Ni(1)-S(11)	2.1441(7)	S(13)-C(12)	1.633(2)
Ni(1)-S(15)	2.149(2)	S(14)-C(12)	1.739(2)
Ni(1)-S(15)	2.149(2)	S(14)-C(13)	1.725(2)
S(11)-C(11)	1.686(2)	S(15)-C(13)	1.687(2)
S(12)-C(11)	1.734(2)	C(11)-C(13)	1.397(2)
Ni(2)-S(21)	2.162(2)	S(25)-C(23)	1.685(2)
Ni(2)-S(25)	2.148(2)	S(26)-C(24)	1.687(2)
Ni(2)-S(26)	2.159(3)	S(27)-C(24)	1.746(2)
Ni(2)-S(30)	2.163(2)	S(27)-C(25)	1.721(2)
S(21)-C(21)	1.695(3)	S(28)-C(25)	1.653(2)
S(22)-C(21)	1.738(2)	S(29)-C(25)	1.726(2)
S(22)-C(22)	1.749(2)	S(29)-C(26)	1.741(2)
S(23)-C(22)	1.632(2)	S(30)-C(26)	1.697(2)
S(24)-C(22)	1.718(2)	C(21)-C(23)	1.395(3)
S(24)-C(23)	1.729(2)	C(24)-C(26)	1.388(2)
Ni(3)-S(31)	2.151(2)	S(35)-C(33)	1.691(8)
Ni(3)-S(35)	2.155(6)	S(36)-C(34)	1.703(8)
Ni(3)-S(36)	2.158(6)	S(37)-C(34)	1.733(8)
Ni(3)-S(40)	2.159(6)	S(37)-C(35)	1.736(7)
S(31)-C(31)	1.685(6)	S(38)-C(35)	1.640(8)
S(32)-C(31)	1.735(9)	S(39)-C(35)	1.722(8)
S(32)-C(32)	1.729(8)	S(39)-C(36)	1.726(8)
S(33)-C(32)	1.632(9)	S(40)-C(36)	1.704(8)
S(34)-C(32)	1.738(8)	C(31)-C(33)	1.395(8)
S(34)-C(33)	1.732(8)	C(34)-C(36)	1.388(8)
N(1)-C(41)	1.464(8)	N(3)-C(51)	1.13(1)
N(1)-C(42)	1.48(1)	C(51)-C(52)	1.45(1)
N(1)-C(43)	1.48(1)		
S(11)-Ni(1)-S(15)	92.70(5)	S(12)-C(12)-S(13)	123.6(1)
C(11)-S(12)-C(12)	97.80(8)	S(12)-C(12)-S(14)	113.4(1)
C(12)-S(14)-C(13)	97.5(1)	S(13)-C(12)-S(14)	123.0(1)
S(11)-C(11)-S(12)	123.9(1)	S(14)-C(13)-S(15)	123.9(1)
S(11)-C(11)-C(13)	120.8(1)	S(14)-C(13)-C(11)	116.0(1)
S(12)-C(11)-C(13)	115.3(1)	S(15)-C(13)-C(11)	120.1(1)
S(21)-Ni(2)-S(25)	92.45(9)	S(22)-C(22)-S(24)	113.0(1)
S(21)-Ni(2)-S(26)	88.39(9)	S(23)-C(22)-S(24)	122.5(1)
S(21)-Ni(2)-S(30)	178.4(1)	S(24)-C(23)-S(25)	123.4(1)
S(25)-Ni(2)-S(26)	178.0(1)	S(24)-C(23)-C(21)	115.7(1)
S(25)-Ni(2)-S(30)	86.17(8)	S(25)-C(23)-C(21)	120.8(1)
S(26)-Ni(2)-S(30)	93.01(9)	S(26)-C(24)-S(27)	123.7(1)
C(21)-S(22)-C(22)	97.5(1)	S(26)-C(24)-C(26)	121.8(1)
C(22)-S(24)-C(23)	98.3(1)	S(27)-C(24)-C(26)	114.5(1)
C(24)-S(27)-C(25)	98.1(1)	S(27)-C(25)-S(28)	123.1(1)
C(25)-S(29)-C(26)	97.2(1)	S(27)-C(25)-S(29)	113.8(1)
S(21)-C(21)-S(22)	124.4(1)	S(28)-C(25)-S(29)	123.2(1)
S(21)-C(21)-C(23)	120.2(1)	S(29)-C(26)-S(30)	123.2(1)
S(22)-C(21)-C(23)	115.4(1)	S(29)-C(26)-C(24)	116.4(1)
S(22)-C(22)-S(23)	124.5(1)	S(30)-C(26)-C(24)	120.4(1)
S(31)-Ni(3)-S(35)	92.8(2)	S(32)-C(32)-S(34)	113.3(4)
S(31)-Ni(3)-S(36)	86.9(2)	S(33)-C(32)-S(34)	121.8(5)
S(31)-Ni(3)-S(40)	177.1(2)	S(34)-C(33)-S(35)	123.3(4)
S(35)-Ni(3)-S(36)	178.4(2)	S(34)-C(33)-C(31)	116.0(5)
S(35)-Ni(3)-S(40)	87.3(2)	S(35)-C(33)-C(31)	120.6(5)
S(36)-Ni(3)-S(40)	93.1(2)	S(36)-C(34)-S(37)	123.3(4)
C(31)-S(32)-C(32)	97.9(4)	S(36)-C(34)-C(36)	121.1(5)
C(32)-S(34)-C(33)	97.5(4)	S(37)-C(34)-C(36)	115.6(5)
C(34)-S(37)-C(35)	97.6(4)	S(37)-C(35)-S(38)	123.6(4)
C(35)-S(39)-C(36)	98.1(4)	S(37)-C(35)-S(39)	113.0(4)
S(31)-C(31)-S(32)	124.0(4)	S(38)-C(35)-S(39)	123.4(4)
S(31)-C(31)-C(33)	120.7(5)	S(39)-C(36)-S(40)	123.8(4)
S(32)-C(31)-C(33)	115.3(5)	S(39)-C(36)-C(34)	115.7(5)
S(32)-C(32)-S(33)	124.9(5)	S(40)-C(36)-C(34)	120.6(5)
C(41)-N(1)-C(42)	110.7(6)	C(42)-N(1)-C(43)	111.1(7)
C(41)-N(1)-C(43)	112.4(6)	N(3)-C(51)-C(52)	179.5(9)

(40) (a) Williams, J. M.; Wang, H. H.; Emge, T. J.; Geiser, U.; Beno, M. A.; Leung, P. C. W.; Carlson, K. D.; Thorn, R. J.; Schultz, A. J.; Whangbo, M.-H. In *Progress in Inorganic Chemistry*; Lippard, S. J., Ed., Interscience: New York, 1987, Vol. 35, p 173. (b) Since overlap is explicitly included in extended Hückel calculations, these interaction energies ( $\beta$ ) should not be confused with the conventional transfer integrals ( $t$ ). Although the two quantities are obviously related and have the same physical meaning, the absolute values of  $\beta$  are somewhat greater than those of  $t$ .

the viewpoint of the oxidation states, the two Ni(dmit)<sub>2</sub> units of the dimers should be considered as [Ni(dmit)<sub>2</sub>]<sup>-1/2</sup> and the single units inbetween the dimers as neutral.

Recently, Cornelissen *et al.*<sup>41</sup> have reported two different Ni(dmit)<sub>2</sub> salts with a divalent closed-shell cation, [Me<sub>3</sub>N(CH<sub>2</sub>)<sub>4</sub>-NMe<sub>3</sub>][Ni(dmit)<sub>2</sub>]<sub>2</sub>·2dmf (dmf = *N,N*-dimethylformamide) and [Me<sub>3</sub>N(CH<sub>2</sub>)<sub>4</sub>NMe<sub>3</sub>][Ni(dmit)<sub>2</sub>]<sub>2</sub>·2MeCN. The repeat unit of

(41) Cornelissen, J. P.; Müller, E.; Vaassens, P. H. S.; Haasnoot, J. G.; Reedijk, J.; Cassoux, P. *Inorg. Chem.* 1992, 31, 2241-2248.

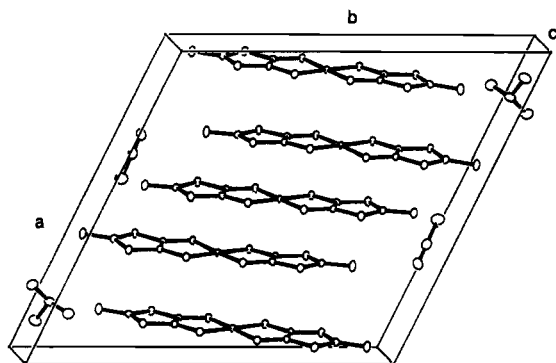


Figure 12. Unit cell of  $(\text{NHMe}_2)_2[\text{Ni}(\text{dmit})_2]_5 \cdot 2\text{MeCN}$  (3).

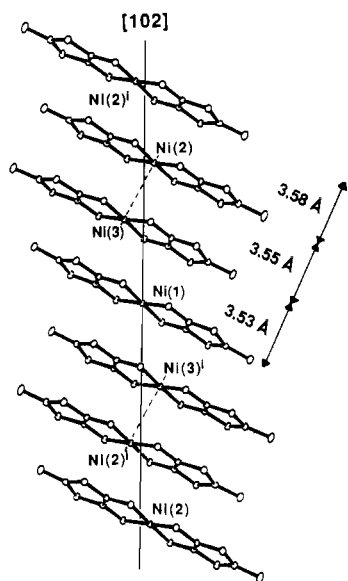


Figure 13. Stacking mode in  $(\text{NHMe}_2)_2[\text{Ni}(\text{dmit})_2]_5 \cdot 2\text{MeCN}$  (3).

the acceptor layers in both compounds contains five  $\text{Ni}(\text{dmit})_2$  units with an overall charge of  $-2$ . However, there are subtle differences in the crystal structures of the two compounds. Whereas the first one contains two weak dimers and a single molecule in the repeat unit of the layer, the second one contains a weak dimer and a weak trimer. Our calculations show that  $[\text{Me}_3\text{N}(\text{CH}_2)_4\text{NMe}_3][\text{Ni}(\text{dmit})_2]_5 \cdot 2\text{dmf}$  is completely analogous to 3; i.e., it can be described as a series of weakly interacting single electrons at the dimers. In the case of  $[\text{Me}_3\text{N}(\text{CH}_2)_4\text{NMe}_3][\text{Ni}(\text{dmit})_2]_5 \cdot 2\text{MeCN}$ , the intradimer and intratrimer interactions are quite sizable ( $\beta_{\text{LUMO-LUMO}} \sim 0.28$  eV) but all other interactions are much weaker. Both the dimer and the trimer have a low-lying empty level quite similar in energy. Thus, from the electronic viewpoint this system can be described as a series of weakly interacting single electrons located at the dimers and trimers. Since the low-lying acceptor orbitals are delocalized inside the dimers or trimers,  $[\text{Me}_3\text{N}(\text{CH}_2)_4\text{NMe}_3][\text{Ni}(\text{dmit})_2]_5 \cdot 2\text{MeCN}$  can be considered as containing  $[\text{Ni}(\text{dmit})_2]^{-1/2}$  and  $[\text{Ni}(\text{dmit})_2]^{-1/3}$  units in contrast with  $[\text{Me}_3\text{N}(\text{CH}_2)_4\text{NMe}_3][\text{Ni}(\text{dmit})_2]_5 \cdot 2\text{dmf}$  and 3, which contain  $[\text{Ni}(\text{dmit})_2]^{-1/2}$  and neutral units.

$(\text{NH}_2\text{Me}_2)_{0.5}[\text{Ni}(\text{dmit})_2]$  (4). Needlelike single crystals of this phase have been obtained by electrocrystallization, or by just leaving a solution of  $(\text{NH}_2\text{Me}_2)[\text{Ni}(\text{dmit})_2]$  in air. Both samples have been characterized as identical by X-ray diffraction methods (Figure 2; Tables 2 and 6). Bond lengths and angles are listed in Table 12. As in 1, the  $\text{Ni}(\text{dmit})_2$  units are practically planar (deviations of the atoms to their least-squares plane less than  $0.02$  Å). Likewise, the N atom of the  $(\text{NH}_2\text{Me}_2)^+$  cation is close to the center of symmetry ( $1; 0; 1/2$ ) and thus these cations are disordered and statistically (50%–50%) distributed over two groups of general positions related through the center of symmetry. Hence, the  $x = 0.5$ , or 1:2 stoichiometry<sup>22</sup> of  $(\text{NH}_2\text{Me}_2)_{0.5}[\text{Ni}(\text{dmit})_2]$  is ascertained.

Table 12. Bond Lengths (Å) and Angles (deg) for  $(\text{NH}_2\text{Me}_2)_{0.5}[\text{Ni}(\text{dmit})_2]$  (4)

Ni–S(1)	2.1582(9)	S(5)–C(3)	1.705(3)
Ni–S(5)	2.1669(9)	S(6)–C(4)	1.696(3)
Ni–S(6)	2.1591(9)	S(7)–C(4)	1.733(3)
Ni–S(10)	2.1593(9)	S(7)–C(5)	1.724(3)
S(1)–C(1)	1.707(3)	S(8)–C(5)	1.647(3)
S(2)–C(1)	1.746(3)	S(9)–C(5)	1.723(3)
S(2)–C(2)	1.724(3)	S(9)–C(6)	1.741(3)
S(3)–C(2)	1.657(3)	S(10)–C(6)	1.693(3)
S(4)–C(2)	1.724(3)	C(1)–C(3)	1.361(4)
S(4)–C(3)	1.748(3)	C(4)–C(6)	1.379(5)
N <sup>a</sup> –C(11) <sup>a</sup>	1.54(2)	N <sup>a</sup> –C(12) <sup>a</sup>	1.47(2)
S(1)–Ni–S(5)	93.28(3)	S(2)–C(2)–S(4)	113.8(2)
S(1)–Ni–S(6)	86.38(3)	S(3)–C(2)–S(4)	123.9(2)
S(1)–Ni–S(10)	177.35(4)	S(4)–C(3)–S(5)	122.8(2)
S(5)–Ni–S(6)	179.36(4)	S(4)–C(3)–C(1)	115.6(2)
S(5)–Ni–S(10)	87.66(3)	S(5)–C(3)–C(1)	121.6(2)
S(6)–Ni–S(10)	92.70(3)	S(6)–C(4)–S(7)	122.9(2)
C(1)–S(2)–C(2)	97.1(2)	S(6)–C(4)–C(6)	121.0(3)
C(2)–S(4)–C(3)	97.3(2)	S(7)–C(4)–C(6)	116.1(2)
C(4)–S(7)–C(5)	97.1(2)	S(7)–C(5)–S(8)	121.9(2)
C(5)–S(9)–C(6)	97.1(2)	S(7)–C(5)–S(9)	114.1(2)
S(1)–C(1)–S(2)	122.3(2)	S(8)–C(5)–S(9)	123.9(2)
S(1)–C(1)–C(3)	121.5(2)	S(9)–C(6)–S(10)	123.3(2)
S(2)–C(1)–C(3)	116.2(3)	S(9)–C(6)–C(4)	115.6(3)
S(2)–C(2)–S(3)	122.3(2)	S(10)–C(6)–C(4)	121.0(3)
C(11) <sup>a</sup> –N <sup>a</sup> –C(12) <sup>a</sup>	114(1)		

<sup>a</sup> Structure occupation factor 0.5.

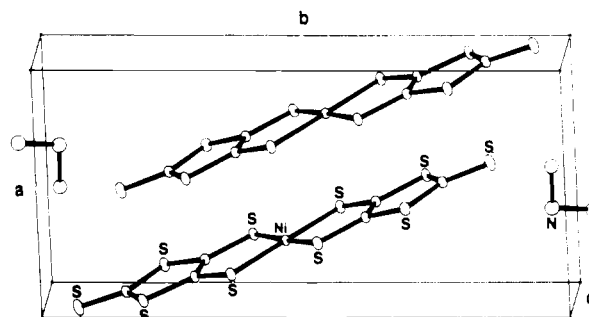


Figure 14. Unit cell of  $(\text{NH}_2\text{Me}_2)_{0.5}[\text{Ni}(\text{dmit})_2]$  (4). The  $(\text{NH}_2\text{Me}_2)^+$  cations are disordered; for clarity only one of the two groups of positions statistically occupied is drawn.

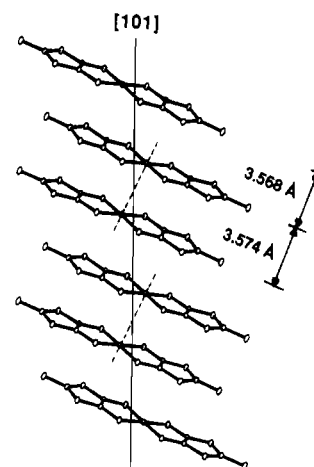


Figure 15. Stacking mode in  $(\text{NH}_2\text{Me}_2)_{0.5}[\text{Ni}(\text{dmit})_2]$  (4).

The structure consists of  $\text{Ni}(\text{dmit})_2$  layers parallel to the (010) plane separated by sheets of  $(\text{NH}_2\text{Me}_2)^+$  cations along the [010] direction. The  $\text{Ni}(\text{dmit})_2$  units are stacked along the [101] direction and weakly dimerized (Figure 15). Within a stack, the distances between the mean planes of two  $\text{Ni}(\text{dmit})_2$  units are 3.574 and 3.568 Å, alternately. Short ( $<3.7$  Å) intermolecular intrastack and interstack sulfur...sulfur contacts

are observed between neighboring Ni(dmit)<sub>2</sub> molecules (supplementary material, Table S13).

Single-crystal, temperature-dependent conductivity measurements along the needle axis show a semiconducting behavior (room-temperature conductivity  $\sigma_{RT} = 0.1 \text{ S}\cdot\text{cm}^{-1}$ ; activation energy  $E_a = 0.21 \text{ eV}$ ).

There are six different types of Ni(dmit)<sub>2</sub>···Ni(dmit)<sub>2</sub> interactions associated with sulfur-sulfur distances smaller than 3.7 Å (supplementary material, Table S13). The intradimer interaction is by far the strongest ( $\beta_{\text{LUMO-LUMO}} = 0.29 \text{ eV}$ ). The interdimer interaction along the stacking direction is about four times smaller ( $\beta_{\text{LUMO-LUMO}} = 0.07 \text{ eV}$ ) and all the interstack interactions are very weak ( $\beta_{\text{LUMO-LUMO}} < 0.01 \text{ eV}$ ). It is interesting to compare these results with those for (2). The interstack LUMO-LUMO interactions are very weak in both compounds which confers them a strong one-dimensional character. The essential difference is to be found in the intrastack interactions. Whereas in (2) the intradimer and interdimer interactions are quite sizable and very similar ( $\beta_{\text{LUMO-LUMO}} = 0.24$  and  $0.23 \text{ eV}$ ), in (4) the intradimer interaction is even stronger but the interdimer interaction is four times smaller. This alternation of strong and weak interactions along the stacks leads to flat bands and hence the electrons in 4 will be localized. This explains the activated conductivity behavior. In contrast, the similar strength of the intra- and interdimer interactions in 2 leads to the delocalization of the electrons along the stack, which explains the metallic-type conductivity.

(NH<sub>3</sub>Me)<sub>2</sub>[M(dmit)<sub>2</sub>]<sub>2</sub>·2MeCN (5). Plateletlike crystals have been obtained by electrocrystallization and characterized by X-ray diffraction methods as the (NH<sub>3</sub>Me)<sub>2</sub>[M(dmit)<sub>2</sub>]<sub>2</sub>·2MeCN phase with the same stoichiometry as in 3. (Figure 3; Tables 3 and 7). Bond lengths and angles are listed in Table 13. Compound 5 is isostructural with compound 3 as far as the anions are concerned, but contrary to what is observed in 3, the cations are disordered in 5. Bearing this in mind, the unit cell is similar to that shown in Figure 12. Likewise, the structure of 5 is very similar to that of 3 and consists of Ni(dmit)<sub>2</sub> layers parallel to the (010) plane separated by sheets of (NH<sub>3</sub>Me)<sup>+</sup> cations and solvent molecules along the [010] direction, and the Ni(dmit)<sub>2</sub> units are stacked along the [102] direction following the same pattern (supplementary material, Figure SF2, Table S14).

Single-crystal, temperature-dependent conductivity measurements along the longest axis of the platelets show a semiconducting behavior (room-temperature conductivity  $\sigma_{RT} = 1.5 \text{ S}\cdot\text{cm}^{-1}$ ; activation energy  $E_a = 0.20 \text{ eV}$ ).

**Comparison of Structures and Properties of Compounds 1–5.** The compared band structure calculations have shown that very subtle differences in the structure may result in large differences in the properties. We may also propose a qualitative structure-properties relationship by comparing the overlap of the Ni(dmit)<sub>2</sub> molecules in compounds 1–5.

In compounds exhibiting a 1:2 stoichiometry such as 1, 2, and 4, the Ni(dmit)<sub>2</sub> entities are weakly dimerized along the stacking direction. Within a dimer of compounds 1 or 2, the Ni(dmit)<sub>2</sub> units are shifted in the transverse direction, and the interdimer shear results in an essentially longitudinal offset (Figure 16), allowing sizable  $\pi$  overlap and possibly explaining the higher conductivity. In compounds exhibiting a 2:5 stoichiometry such as 3 and 5, alternating dimers and single molecules are observed along the stacking direction. A similar intradimer transverse offset is observed, but interdimer and dimer-single molecule shears now result in a longitudinal and transverse offset. Likewise, in 4 the sole interdimer shear results in a similar situation. In these latter cases the  $\pi$  overlap should be much smaller, resulting in smaller conductivities.

These observations can be put in a somewhat more quantitative basis by using the above-mentioned  $\beta_{\text{LUMO-LUMO}}$  interaction energies. It is remarkable that the intradimer interaction energies in 1–5 are rather similar ( $\beta_{\text{LUMO-LUMO}} = 0.24$ – $0.29 \text{ eV}$ ). This seems to be the case not only for salts containing Ni(dmit)<sub>2</sub> dimers

**Table 13.** Bond Lengths (Å) and Angles (deg) for (NH<sub>3</sub>Me)<sub>2</sub>[Ni(dmit)<sub>2</sub>]<sub>2</sub>·2MeCN (5)

Ni(1)–S(11)	2.146(2)	S(12)–C(12)	1.74(1)
Ni(1)–S(11)	2.146(2)	S(13)–C(12)	1.63(1)
Ni(1)–S(15)	2.147(2)	S(14)–C(12)	1.73(1)
Ni(1)–S(15)	2.147(2)	S(14)–C(13)	1.71(1)
S(11)–C(11)	1.68(1)	S(15)–C(13)	1.701(9)
S(12)–C(11)	1.74(1)	C(11)–C(13)	1.39(1)
Ni(2)–S(21)	2.151(3)	S(25)–C(23)	1.67(1)
Ni(2)–S(25)	2.147(3)	S(26)–C(24)	1.72(1)
Ni(2)–S(26)	2.160(3)	S(27)–C(24)	1.74(1)
Ni(2)–S(30)	2.159(3)	S(27)–C(25)	1.74(1)
S(21)–C(21)	1.67(1)	S(28)–C(25)	1.63(1)
S(22)–C(21)	1.75(1)	S(29)–C(25)	1.72(1)
S(22)–C(22)	1.74(1)	S(29)–C(26)	1.72(1)
S(23)–C(22)	1.61(1)	S(30)–C(26)	1.70(1)
S(24)–C(22)	1.74(1)	C(21)–C(23)	1.40(1)
S(24)–C(23)	1.73(1)	C(24)–C(26)	1.36(1)
S(23)–C(22)	1.61(1)	S(30)–C(26)	1.70(1)
S(24)–C(22)	1.74(1)	C(21)–C(23)	1.40(1)
S(24)–C(23)	1.73(1)	C(24)–C(26)	1.36(1)
Ni(3)–S(31)	2.155(3)	S(35)–C(33)	1.70(1)
Ni(3)–S(35)	2.151(3)	S(36)–C(34)	1.696(9)
Ni(3)–S(36)	2.157(3)	S(37)–C(34)	1.75(1)
Ni(3)–S(40)	2.152(3)	S(37)–C(35)	1.75(1)
S(31)–C(31)	1.68(1)	S(38)–C(35)	1.63(1)
S(32)–C(31)	1.74(1)	S(39)–C(35)	1.72(1)
S(32)–C(32)	1.71(1)	S(39)–C(36)	1.731(9)
S(33)–C(32)	1.63(1)	S(40)–C(36)	1.69(1)
S(34)–C(32)	1.74(1)	C(31)–C(33)	1.39(1)
S(34)–C(33)	1.72(1)	C(34)–C(36)	1.38(1)
N(3)–C(51)	1.15(2)	C(51)–C(52)	1.41(2)
N(1) <sup>a</sup> –C(41) <sup>a</sup>	1.42(2)	N(2) <sup>a</sup> –C(42) <sup>a</sup>	1.40(2)
S(11)–Ni(1)–S(15)	92.8(1)	S(12)–C(12)–S(13)	123.2(6)
C(11)–S(12)–C(12)	97.6(5)	S(12)–C(12)–S(14)	122.9(6)
C(12)–S(14)–C(13)	97.6(5)	S(13)–C(12)–S(14)	123.8(6)
S(11)–C(11)–S(12)	123.2(5)	S(14)–C(13)–S(15)	123.7(5)
S(11)–C(11)–C(13)	122.1(7)	S(14)–C(13)–C(11)	117.1(7)
S(12)–C(11)–C(13)	114.7(7)	S(15)–C(13)–C(11)	119.1(7)
S(21)–Ni(2)–S(25)	92.7(1)	S(22)–C(22)–S(24)	113.1(6)
S(21)–Ni(2)–S(26)	87.5(1)	S(23)–C(22)–S(24)	122.0(6)
S(21)–Ni(2)–S(30)	178.9(1)	S(24)–C(23)–S(25)	123.5(5)
S(25)–Ni(2)–S(26)	178.1(1)	S(24)–C(23)–C(21)	116.3(8)
S(25)–Ni(2)–S(30)	86.5(1)	S(25)–C(23)–C(21)	120.1(8)
S(26)–Ni(2)–S(30)	93.3(1)	S(26)–C(24)–S(27)	122.0(5)
C(21)–S(22)–C(22)	98.1(5)	S(26)–C(24)–C(26)	121.9(8)
C(22)–S(24)–C(23)	98.0(5)	S(27)–C(24)–C(26)	116.1(8)
C(24)–S(27)–C(25)	96.8(5)	S(27)–C(25)–S(28)	122.2(7)
C(25)–S(29)–C(26)	97.6(5)	S(27)–C(25)–S(29)	113.2(7)
S(21)–C(21)–S(22)	124.1(5)	S(28)–C(25)–S(29)	124.5(7)
S(21)–C(21)–C(23)	121.3(8)	S(29)–C(26)–S(30)	123.1(6)
S(22)–C(21)–C(23)	114.6(8)	S(29)–C(26)–C(24)	116.2(7)
S(22)–C(22)–S(23)	124.9(6)	S(30)–C(26)–C(24)	120.7(8)
S(31)–Ni(3)–S(35)	92.9(1)	S(32)–C(32)–S(34)	114.1(6)
S(31)–Ni(3)–S(36)	87.0(1)	S(33)–C(32)–S(34)	121.5(6)
S(31)–Ni(3)–S(40)	176.6(1)	S(34)–C(33)–S(35)	123.2(5)
S(35)–Ni(3)–S(36)	178.7(1)	S(34)–C(33)–C(31)	116.8(7)
S(35)–Ni(3)–S(40)	86.8(1)	S(35)–C(33)–C(31)	120.0(8)
S(36)–Ni(3)–S(40)	93.3(1)	S(36)–C(34)–S(37)	122.5(5)
C(31)–S(32)–C(32)	97.3(5)	S(36)–C(34)–C(36)	121.9(8)
C(32)–S(34)–C(33)	96.8(5)	S(37)–C(34)–C(36)	115.6(7)
C(34)–S(37)–C(35)	97.3(5)	S(37)–C(35)–S(38)	123.4(6)
C(35)–S(39)–C(36)	98.3(5)	S(37)–C(35)–S(39)	112.9(6)
S(31)–C(31)–S(32)	123.2(5)	S(38)–C(35)–S(39)	123.7(6)
S(31)–C(31)–C(33)	121.8(7)	S(39)–C(36)–S(40)	123.6(5)
S(32)–C(31)–C(33)	114.9(8)	S(39)–C(36)–C(34)	115.9(7)
S(32)–C(32)–S(33)	124.4(6)	S(40)–C(36)–C(34)	120.4(7)
N(3)–C(51)–C(52)	177(2)		

<sup>a</sup> The (NH<sub>3</sub>Me)<sup>+</sup> cation is statistically distributed over two sets of positions. The structure occupation factor (0.5) was estimated on the basis of the similarity of isotropic temperature factors.

but also for those having regular stacks. For instance, the  $\beta_{\text{LUMO-LUMO}}$  for two adjacent Ni(dmit)<sub>2</sub> units along the regular stacks of TTF[Ni(dmit)<sub>2</sub>]<sub>2</sub><sup>42</sup> and  $\alpha$ -(EDT-TTF)[Ni(dmit)<sub>2</sub>]<sub>2</sub><sup>43</sup> are 0.28 and 0.24 eV, respectively. These results make clear a remarkable tendency of Ni(dmit)<sub>2</sub> toward this type of association

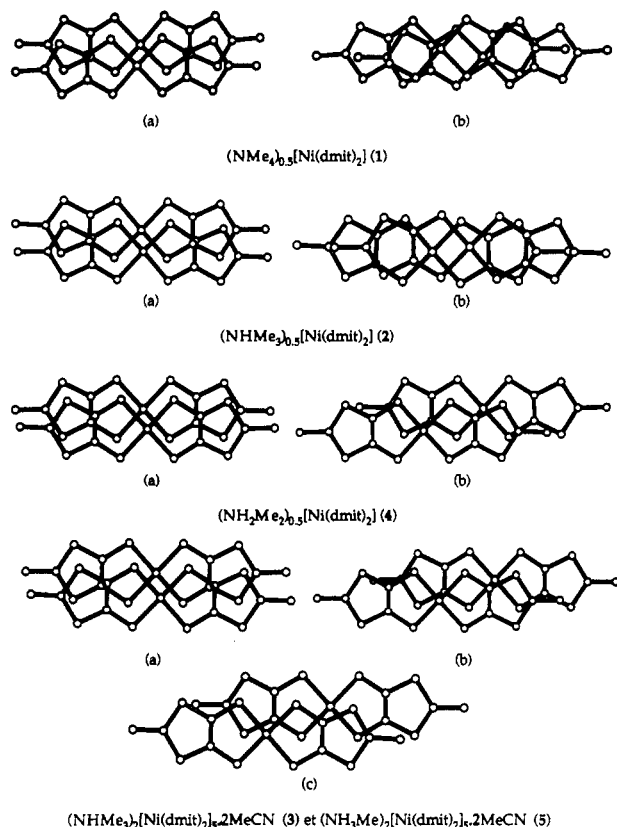


**Figure 16.** Modes of overlap in  $(\text{NH}_4)\text{Me}_{4-x}[\text{Ni}(\text{dmit})_2]$  anion radical salts 1–5: (a) intradimer; (b) interdimer; (c) mode between a dimer and a single  $\text{Ni}(\text{dmit})_2$  molecule in 3 and 5.

in dimers with a transverse slipping. How regularly these dimers are organized along the stacks seems to be controlled in a very subtle way by the nature of the donor. Only when the intra- and interdimer interaction energies along the stacks are sizable and very similar do the salts exhibit metallic conductivity. However, an interesting observation is that similarity of interaction energies does not necessarily mean similarity of overlap modes. Although every pair of adjacent  $\text{Ni}(\text{dmit})_2$  units along the stacks of TTF- $[\text{Ni}(\text{dmit})_2]_2$  and  $\alpha$ -(EDT-TTF) $[\text{Ni}(\text{dmit})_2]$  have a transverse type slipping, those of 1 and 2 are successively of the transverse and longitudinal type, and yet the two types of interaction energies are very similar.

$(\text{NH}_4)[\text{Ni}(\text{dmit})_2] (6)$ . Depending on the nature of the solvent, acetone/nitromethane (1:1) or acetonitrile, two kinds of crystals, platelets or needles, respectively, have been obtained by galvanostatic oxidation of a solution of  $(\text{NBu}_4)[\text{Ni}(\text{dmit})_2]$  in the presence of a very large excess of  $(\text{NH}_4)\text{Cl}$ . Only the plateletlike crystals could be characterized by X-ray diffraction [monoclinic, space group  $C2/c$ ,  $a = 37.839(9)$  Å,  $b = 11.174(4)$  Å,  $c = 11.801(5)$  Å,  $\beta = 104.88(2)^\circ$ ,  $V = 4823(3)$  Å<sup>3</sup>; to be compared with<sup>19</sup> monoclinic, space group  $C2/c$ ,  $a = 37.940(3)$  Å,  $b = 11.186(1)$  Å,  $c = 11.840(1)$  Å,  $\beta = 104.93(3)^\circ$ ,  $V = 4855(1)$  Å<sup>3</sup>]. The crystal structure is similar to the one previously reported,<sup>19</sup> at least as far as the stacking mode of the  $\text{Ni}(\text{dmit})_2$  anions is concerned. The discrepancies observed on parameters  $a$  and  $c$  may be due to variations in the solvent and/or cation contents. Actually, as it happened in the former study,<sup>19</sup> our attempts to locate the cations (and possibly solvent molecules) failed and, therefore, the actual stoichiometry of this phase is still unknown.

Temperature-dependent conductivity measurements along the axis of the needles or the longest axis of the platelets show in both cases a semiconducting behavior (room temperature conductivity  $\sigma_{\text{RT}} = 0.2$  S·cm<sup>-1</sup> (needle) and  $0.7$  S·cm<sup>-1</sup> (platelets), with

activation energy  $E_a \approx 0.1$  eV in both cases). These results are in good agreement with the previous values<sup>19</sup> for the semiconducting samples; however, we did not observe the metallic phase with  $\sigma_{\text{RT}} = 50$  S·cm<sup>-1</sup> mentioned in the previous study.<sup>19</sup> The semiconducting behavior of the platelet-shaped crystals is retained under a pressure of 10 kbar.<sup>20</sup>

$(\text{NHMe}_3)[\text{Pt}(\text{dmit})_2]_3 \cdot \text{MeCN} (7)$ . This compound is the single platinum compound of the  $(\text{NH}_4)\text{Me}_{4-x}[\text{M}(\text{dmit})_2]$  series which could be characterized by X-ray diffraction methods (Figure 4; Tables 3 and 8). Bond lengths and angles are listed in Table 14. Its 1:3 stoichiometry is rather unusual (although it should be noted that the donor–acceptor complex TTF $[\text{Pt}(\text{dmit})_2]_3$  has been reported previously<sup>42</sup>). The asymmetric unit contains three crystallographically independent  $\text{Pt}(\text{dmit})_2$  entities, one  $(\text{NHMe}_3)^+$  cation, and one MeCN molecule, both being not disordered; the content of the unit cell is shown in Figure 17. The  $\text{Pt}(\text{dmit})_2$  entities are paired, forming two crystallographically independent dimers with  $\text{Pt}(1)\text{--Pt}(2)$  and  $\text{Pt}(3)\text{--Pt}(3)^i$  bond lengths of 3.01 and 3.12 Å, respectively [ $\text{Pt}(3)$  and  $\text{Pt}(3)^i$  refer to two crystallographically equivalent Pt atoms, superscript  $i$  indicates an inversion through a center of symmetry]. The strong Pt–Pt interactions and the ensuing S··S repulsions are also evidenced by the perfectly eclipsed overlap of two  $\text{Pt}(\text{dmit})_2$  entities within a dimer (*vide infra*), which results in an angle of  $3.9^\circ$  between the dmit planes for the  $\text{Pt}(1)(\text{dmit})_2$  entity,  $8.7^\circ$  for the  $\text{Pt}(2)(\text{dmit})_2$  entity, and  $6.9^\circ$  for the  $\text{Pt}(3)(\text{dmit})_2$  and the  $\text{Pt}(3)^i(\text{dmit})_2$  entities. The structure consists of layers of  $[\text{Pt}(\text{dmit})_2]_2$  dimers parallel to the (010) plane separated by sheets of  $(\text{NHMe}_3)^+$  cations and MeCN molecules along the [010] direction. The  $[\text{Pt}(\text{dmit})_2]_2$  dimers are stacked along the [001] direction (Figure 18). As usual, short (<3.7 Å), intermolecular sulfur··sulfur distances are observed (supplementary material, Table S15). Within a dimer, the  $\text{Pt}(\text{dmit})_2$  units are perfectly eclipsed and only a longitudinal offset is observed in the interdimer overlap, resulting thus in a situation enhancing  $\pi$  interactions along the stacks (Figure 19).

The crystals used for temperature-dependent conductivity measurements were very brittle, long, and thin platelets (typically  $3 \times 0.2 \times 0.01$  mm<sup>3</sup>). Given the brittleness of this sample, we were not able to carry out conductivity measurements under pressure. The room-temperature conductivity, 140 S·cm<sup>-1</sup>, is the highest observed in  $\text{Pt}(\text{dmit})_2$  compounds and remains almost constant down to 180 K. Below this temperature, the compound becomes semiconducting.<sup>15</sup> This behavior is to be compared to that of  $(\text{NMe}_4)[\text{Pt}(\text{dmit})_2]_2$ , which exhibits similar features ( $\sigma_{\text{RT}} = 10$  S·cm<sup>-1</sup>; pseudometal-to-insulator transition temperature 220 K).<sup>44</sup> In the present case, substituting a H atom for a methyl group results in a change in the stoichiometry (from 1:2 to 1:3) and an increase in the conductivity. It is also interesting to note that strong dimerization effects in  $\text{M}(\text{dmit})_2$  systems with  $\text{M} = \text{Pd}$  or  $\text{Pt}$ , such as  $(\text{NBu}_4)_x[\text{Pd}(\text{dmit})_2]$  ( $x = 0.33, 0.5$ ),<sup>45</sup>  $\delta$ -TTF- $[\text{Pd}(\text{dmit})_2]_2$ ,<sup>46</sup>  $\beta$ -( $\text{NMe}_4$ ) $[\text{Pd}(\text{dmit})_2]_2$ ,<sup>10</sup>  $(\text{NMe}_4)[\text{Pt}(\text{dmit})_2]_2$ ,<sup>44</sup> and (7), do not prevent these compounds from exhibiting high conductivities.

The energy dispersion curves calculated for  $(\text{NHMe}_3)[\text{Pt}(\text{dmit})_2]_3 \cdot \text{MeCN}$  are shown in Figure 20.

To the six  $\text{Pt}(\text{dmit})_2$  units in the unit cell correspond six HOMO bands and six LUMO bands. A remarkable difference with the dispersion curves of (1) and (2) (Figure 10) is that a group of three LUMO bands are lower in energy than a group of three HOMO bands. As has been analyzed elsewhere,<sup>8,38</sup> the HOMO and LUMO of  $\text{M}(\text{dmit})_2$  ( $\text{M} = \text{Ni}, \text{Pd}, \text{Pt}$ ) are quite close in energy ( $\sim 0.40$  eV) and are mainly ligand in character. If there is a real dimerization of the  $\text{M}(\text{dmit})_2$  molecules, the splitting between the two combinations originating from each of these two

(42) Bousseau, M.; Valade, L.; Legros, J.-P.; Cassoux, P.; Garbauskas, M.; Interrante, L. V. *J. Am. Chem. Soc.* **1986**, *108*, 1908–1916.

(43) Kato, R.; Kobayashi, H.; Kobayashi, A.; Naito, T.; Tamura, M.; Tajima, H.; Kuroda, H. *Chem. Lett.* **1989**, 1839–1842.

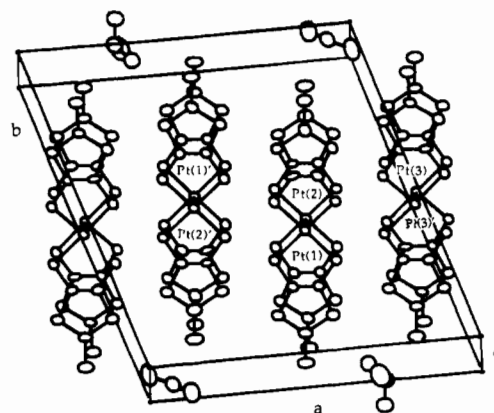
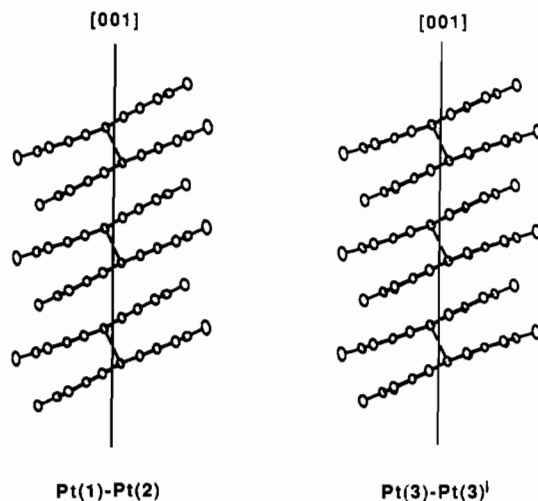
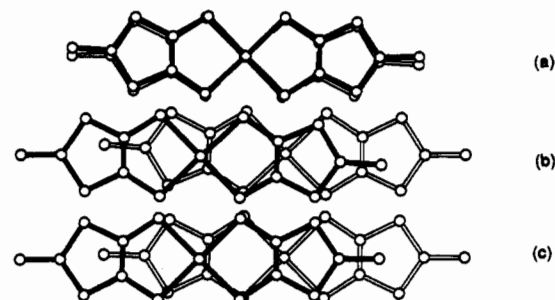
(44) Kobayashi, A.; Miyamoto, A.; Kobayashi, H.; Clark, R. A.; Underhill, A. E. *J. Mater. Chem.* **1991**, *1*, 827–830.

(45) Legros, J.-P.; Valade, L.; Cassoux, P. *Synth. Met.* **1988**, *27*, B347–B352.

(46) Legros, J.-P.; Valade, L. *Solid State Commun.* **1988**, *68*, 599–604.

**Table 14.** Bond Lengths (Å) and Angles (deg) for (NHMe<sub>3</sub>)<sub>3</sub>[Pt(dmit)<sub>2</sub>]<sub>3</sub>·MeCN (7) Where the Superscript i Indicates Inversion through a Symmetry Center

Pt(1)-Pt(2)	3.0147(8)	Pt(3)-Pt(3) <sup>i</sup>	3.122(1)
Pt(1)-S(11)	2.288(4)	S(15)-C(13)	1.70(1)
Pt(1)-S(15)	2.284(5)	S(16)-C(14)	1.68(1)
Pt(1)-S(16)	2.293(5)	S(17)-C(14)	1.73(2)
Pt(1)-S(20)	2.293(4)	S(17)-C(15)	1.73(1)
S(11)-C(11)	1.69(2)	S(18)-C(15)	1.63(2)
S(12)-C(11)	1.74(1)	S(19)-C(15)	1.74(2)
S(12)-C(12)	1.74(2)	S(19)-C(16)	1.73(1)
S(13)-C(12)	1.62(2)	S(20)-C(16)	1.71(2)
S(14)-C(12)	1.75(2)	C(11)-C(13)	1.37(2)
S(14)-C(13)	1.75(2)	C(14)-C(16)	1.38(2)
Pt(2)-S(21)	2.290(5)	S(25)-C(23)	1.71(2)
Pt(2)-S(25)	2.295(4)	S(26)-C(24)	1.73(2)
Pt(2)-S(26)	2.295(4)	S(27)-C(24)	1.71(1)
Pt(2)-S(30)	2.300(5)	S(27)-C(25)	1.74(2)
S(21)-C(21)	1.75(1)	S(28)-C(25)	1.62(2)
S(22)-C(21)	1.73(1)	S(29)-C(25)	1.75(2)
S(22)-C(22)	1.75(1)	S(29)-C(26)	1.75(2)
S(23)-C(22)	1.61(2)	S(30)-C(26)	1.69(1)
S(24)-C(22)	1.73(2)	C(21)-C(23)	1.31(2)
S(24)-C(23)	1.72(1)	C(24)-C(26)	1.38(2)
Pt(3)-S(31)	2.291(4)	S(35)-C(33)	1.68(1)
Pt(3)-S(35)	2.277(5)	S(36)-C(36)	1.72(2)
Pt(3)-S(36)	2.285(4)	S(37)-C(35)	1.74(2)
Pt(3)-S(40)	2.293(5)	S(37)-C(36)	1.74(1)
S(31)-C(31)	1.69(2)	S(38)-C(35)	1.63(1)
S(32)-C(31)	1.73(1)	S(39)-C(34)	1.73(2)
S(32)-C(32)	1.73(2)	S(39)-C(35)	1.72(1)
S(33)-C(32)	1.64(1)	S(40)-C(34)	1.71(1)
S(34)-C(32)	1.72(1)	C(31)-C(33)	1.41(2)
S(34)-C(33)	1.73(2)	C(34)-C(36)	1.38(2)
N(1)-C(41)	1.47(3)	N(1)-C(43)	1.47(3)
N(1)-C(42)	1.48(3)		
N(3)-C(51)	1.12(3)	C(51)-C(52)	1.46(4)
S(11)-Pt(1)-S(15)	90.0(2)	S(12)-C(12)-S(14)	112.0(9)
S(11)-Pt(1)-S(16)	89.6(2)	S(13)-C(12)-S(14)	124(1)
S(11)-Pt(1)-S(20)	173.1(2)	S(14)-C(13)-S(15)	120.6(9)
S(15)-Pt(1)-S(16)	174.5(2)	S(14)-C(13)-C(11)	115(1)
S(15)-Pt(1)-S(20)	90.0(2)	S(15)-C(13)-C(11)	124(1)
S(16)-Pt(1)-S(20)	89.7(2)	S(16)-C(14)-S(17)	120.7(9)
C(11)-S(12)-C(12)	98.1(8)	S(16)-C(14)-C(16)	124(1)
C(12)-S(14)-C(13)	98.2(8)	S(17)-C(14)-C(16)	115(1)
C(14)-S(17)-C(15)	97.9(7)	S(17)-C(15)-S(18)	123(1)
C(15)-S(19)-C(16)	97.1(7)	S(17)-C(15)-S(19)	113.1(8)
S(11)-C(11)-S(12)	121.3(9)	S(18)-C(15)-S(19)	123.5(9)
S(11)-C(11)-C(12)	122(1)	S(19)-C(16)-S(20)	121.3(9)
S(12)-C(11)-C(13)	117(1)	S(19)-C(16)-C(14)	117(1)
S(12)-C(12)-S(13)	124(1)	S(20)-C(16)-C(14)	122(1)
S(21)-Pt(2)-S(25)	89.1(1)	S(22)-C(22)-S(24)	112.4(9)
S(21)-Pt(2)-S(26)	90.1(1)	S(23)-C(22)-S(24)	123.9(9)
S(21)-Pt(2)-S(30)	173.0(2)	S(24)-C(23)-S(25)	120.6(9)
S(25)-Pt(2)-S(26)	174.0(1)	S(24)-C(23)-C(21)	116(1)
S(25)-Pt(2)-S(30)	90.2(1)	S(25)-C(23)-C(21)	124(1)
S(26)-Pt(2)-S(30)	89.8(1)	S(26)-C(24)-S(27)	121.3(9)
C(21)-S(22)-C(22)	95.6(8)	S(26)-C(24)-C(26)	121(1)
C(22)-S(24)-C(23)	97.7(7)	S(27)-C(24)-C(26)	118(1)
C(24)-S(27)-C(25)	97.8(7)	S(27)-C(25)-S(28)	123.7(9)
C(25)-S(29)-C(26)	98.1(7)	S(27)-C(25)-S(29)	112.2(8)
S(21)-C(21)-S(22)	118.1(9)	S(28)-C(25)-S(29)	124(1)
S(21)-C(21)-C(23)	123(1)	S(29)-C(26)-S(30)	121.0(9)
S(22)-C(21)-C(23)	119(1)	S(29)-C(26)-C(24)	114(1)
S(22)-C(22)-S(23)	124(1)	S(30)-C(26)-C(24)	125(1)
S(31)-Pt(3)-S(35)	89.7(2)	S(32)-C(32)-S(34)	113.6(8)
S(31)-Pt(3)-S(36)	175.1(2)	S(33)-C(32)-S(34)	122(1)
S(31)-Pt(3)-S(40)	91.4(2)	S(34)-C(33)-S(35)	122.2(9)
S(35)-Pt(3)-S(36)	88.4(2)	S(34)-C(33)-C(31)	115(1)
S(35)-Pt(3)-S(40)	174.3(2)	S(35)-C(33)-C(31)	123(1)
S(36)-Pt(3)-S(40)	90.1(2)	S(39)-C(34)-S(40)	122(1)
C(31)-S(32)-C(32)	97.8(7)	S(39)-C(34)-C(36)	116(1)
C(32)-S(34)-C(33)	98.0(7)	S(40)-C(34)-C(36)	123(1)
C(35)-S(37)-C(36)	97.3(7)	S(37)-C(35)-S(38)	122.7(9)
C(34)-S(39)-C(35)	98.1(8)	S(37)-C(35)-S(39)	112.8(8)
S(31)-C(31)-S(32)	122.3(9)	S(38)-C(35)-S(39)	125(1)
S(31)-C(31)-C(33)	122(1)	S(36)-C(36)-S(37)	120.9(9)
S(32)-C(31)-C(33)	115(1)	S(36)-C(36)-C(34)	123(1)
S(32)-C(32)-S(33)	124.8(9)	S(37)-C(36)-C(34)	116(1)
C(41)-N(1)-C(42)	110(2)	C(42)-N(1)-C(43)	112(2)
C(41)-N(1)-C(43)	111(2)	N(3)-C(51)-C(52)	177(3)

**Figure 17.** Unit cell of (NHMe<sub>3</sub>)<sub>3</sub>[Pt(dmit)<sub>2</sub>]<sub>3</sub>·MeCN (7).**Figure 18.** Stacking mode in (NHMe<sub>3</sub>)<sub>3</sub>[Pt(dmit)<sub>2</sub>]<sub>3</sub>·MeCN (7).**Figure 19.** Modes of overlap in (NHMe<sub>3</sub>)<sub>3</sub>[Pt(dmit)<sub>2</sub>]<sub>3</sub>·MeCN (7): (a) intradimer; (b) interdimer Pt(3)-Pt(3)<sup>i</sup>; (c) interdimer Pt(1)-Pt(2).

orbitals can be large enough to raise the antibonding combination of the HOMOs ( $\Psi^-_{\text{HOMO}}$ ) above the bonding combination of the LUMOs ( $\Psi^+_{\text{LUMO}}$ ). Thus, the presence of real [Pt(dmit)<sub>2</sub>]<sub>2</sub> dimers in 7 leads to the inversion of the HOMO<sup>+</sup> and LUMO<sup>-</sup> bands in Figure 20. Given the 1:3 stoichiometry of this compound, fourteen electrons will be found in the lowest energy bands. Consequently, the Fermi level will be close to the seventh and eighth bands which happen to be HOMO bands. The resulting Fermi surface is shown in Figure 21.

At the  $\Gamma$  point of the Brillouin zone, the Fermi level is below both bands 7 and 8, resulting in a hole pocket. Along the  $\Gamma \rightarrow X$  direction, the Fermi level intersects band 7 but remains below band 8, whereas along the  $\Gamma \rightarrow Z$  direction, the Fermi level intersects both bands 7 and 8, forming an electron pocket around Z. These results suggest two possible explanations of the pseudometal-to-insulator transition observed in this compound at 180 K: (i) at this temperature, an even minute structural modification, within the unit cell but without change in the periodicity, may be sufficient to remove the overlap of bands 7 and 8, resulting thus in an energy gap between both of these

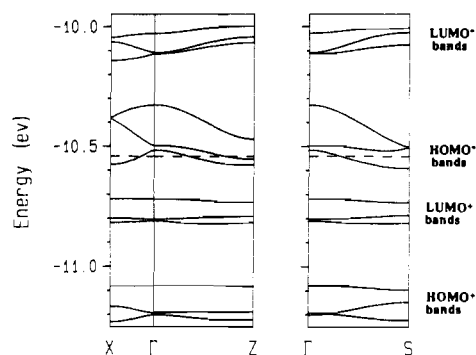


**Figure 20.** Band structure for the  $\text{Pt}(\text{dmit})_2$  slabs in  $(\text{NHMe}_3)[\text{Pt}(\text{dmit})_2]_3 \cdot \text{MeCN}$  (**7**);  $\Gamma$ ,  $X$ ,  $Z$ , and  $S$  refer to the wave vectors  $(0, 0)$ ,  $(a^*/2, 0)$ ,  $(0, c^*/2)$ , and  $(-a^*/2, c^*/2)$ , respectively.

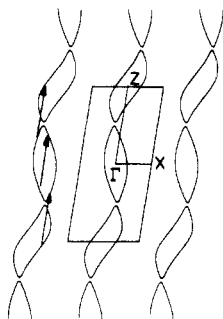


**Figure 21.** Fermi surface of  $(\text{NHMe}_3)[\text{Pt}(\text{dmit})_2]_3 \cdot \text{MeCN}$  (**7**).

bands; (ii) the Fermi surface of Figure 21 exhibits a nesting vector corresponding approximately to a trimerization along  $c$  which could result in a CDW (or even a spin density wave) condensation. One should bear in mind that although the total width of the HOMO<sup>-</sup> bands is similar to those of other metallic salts containing  $\text{M}(\text{dmit})_2$  dimers, like  $\text{Cs}[\text{Pd}(\text{dmit})_2]_2$ ,<sup>39</sup>  $\delta\text{-TTF}[\text{Pd}(\text{dmit})_2]_2$ ,<sup>38</sup> and  $(\text{NMe}_4)[\text{Pt}(\text{dmit})_2]_2$ ,<sup>47</sup> band 7 is quite narrow, so that electronic localization could be competing with the proposed structural instabilities. Structural work at low temperature and X-ray diffuse scattering measurements are clearly needed in order to test these hypotheses.

As shown in Figure 20, the HOMO<sup>-</sup> bands are dispersive but the LUMO<sup>+</sup> bands are very flat. Thus if it were not for the inversion of the HOMO<sup>-</sup> and LUMO<sup>+</sup> bands brought about by the dimerization, this system would not be a good conductor.<sup>8,48</sup> This link between strong dimerization and good conductivity seems to be in contradiction with our analysis of the electronic structure of the  $(\text{NH}_y\text{Me}_{4-y})_x[\text{M}(\text{dmit})_2]$  salts. However, this is not so. Although the Fermi surface of Figure 21 contains closed electron and hole pockets, it can be described as resulting from the superposition and weak hybridization of pairs of warped lines along  $c^*$  (*i.e.* the nesting shown in Figure 21 is a further example of "hidden nesting"<sup>49</sup>). Consequently, **7** will be a metal with better conductivity along the interstack direction and not along the intrastack direction as it is the case for **1** and **2**. This means that the dimerization has brought about a reorganization of the layer so as to increase the interstack interactions and decrease the intrastack interactions. The dominant character of the interstack interactions and the inversion of the HOMO<sup>-</sup> and LUMO<sup>+</sup> bands were already noticed in other metallic systems containing strongly dimerized  $[\text{M}(\text{dmit})_2]_2$  units.<sup>8,38,39,47,48</sup> There-

**Table 15.** Compacted Powder Conductivity Data ( $\text{S}\cdot\text{cm}^{-1}$ ) for the  $(\text{NH}_y\text{Me}_{4-y})_x[\text{M}(\text{dmit})_2]$  Compounds (and Single-Crystal Data for Phases 1–7)

$(\text{NH}_y\text{Me}_{4-y})$	M = Ni	M = Pd	M = Pt
$\text{NHMe}_3$	0.5–1 (140 for <b>2</b> and 0.2 for <b>3</b> )	0.5–1.5	0.5–1 (140 for <b>7</b> )
$\text{NH}_2\text{Me}_2$	0.1–0.5 (0.1 for <b>4</b> )	0.5	0.2–0.5
$\text{NH}_3\text{Me}$	0.1–0.5 (1.5 for <b>5</b> )	0.5	0.5
$\text{NH}_4$	0.04 (0.3 <sup>19</sup> )	0.04	0.08

fore, we conclude that by using appropriately different arrangements both weak and strong dimers of  $\text{M}(\text{dmit})_2$  units can lead to metallic layers.

**Powder Conductivity.** The powder conductivity (and single-crystal conductivity when available) of the  $(\text{NH}_y\text{Me}_{4-y})_x[\text{M}(\text{dmit})_2]$  phases are listed in Table 15. The conductivity does not seem to depend much on the nature of the metal, but decreases when increasing the number  $y$  of H atoms substituted for methyl groups in the  $(\text{NH}_y\text{Me}_{4-y})^+$  cation.

**Conclusions.** The progressive substitution of H for Me in the  $(\text{NH}_y\text{Me}_{4-y})_x[\text{M}(\text{dmit})_2]$  series shows how delicately a small change in the counteranion shape and size affects the crystal packing and hence the electronic and electrical properties.

While  $(\text{NMe}_4)_{0.5}[\text{Ni}(\text{dmit})_2]$  and  $(\text{NHMe}_3)_{0.5}[\text{Ni}(\text{dmit})_2]$  behave as pseudometals down to 90 and 220 K respectively,  $(\text{NH}_2\text{Me}_2)_{0.5}[\text{Ni}(\text{dmit})_2]$  is a semiconductor; furthermore, the pseudometal-to-insulator transition of  $(\text{NMe}_4)_{0.5}[\text{Ni}(\text{dmit})_2]$  cannot result from a CDW instability while such an instability cannot be ruled out for  $(\text{NHMe}_3)_{0.5}[\text{Ni}(\text{dmit})_2]$ .

In the semiconductive 2:5 phases obtained with  $\text{NHMe}_3^+$  and  $\text{NH}_3\text{Me}^+$ , the repeating unit of the stacks of the  $[\text{Ni}(\text{dmit})_2]$  entities is made of two anionic weak dimers  $[\text{Ni}(\text{dmit})_2]_2^-$  and one neutral single molecule  $[\text{Ni}(\text{dmit})_2]^0$ . The same structure is also found for  $[\text{Me}_3\text{N}(\text{CH}_2)_4\text{NMe}_3][\text{Ni}(\text{dmit})_2]_5 \cdot 2\text{dmf}$ ; however, just changing the solvent from dmf to MeCN gives the phase  $[\text{Me}_3\text{N}(\text{CH}_2)_4\text{NMe}_3][\text{Ni}(\text{dmit})_2]_5 \cdot 2\text{MeCN}$ , the stacks of which are made of alternating weak dimers  $[\text{Ni}(\text{dmit})_2]_2^-$  and weak trimers  $[\text{Ni}(\text{dmit})_2]_3^-$ .

Metal–metal interactions also have a strong influence on the nature of the conduction process. Using platinum as the metal in the  $[\text{M}(\text{dmit})_2]$  unit, one obtains a 1:2 phase with  $\text{NMe}_4^+$  and a 1:3 phase with  $\text{NHMe}_3^+$ . In both phases the  $[\text{Pt}(\text{dmit})_2]$  units are associated in dimers through a strong Pt–Pt interaction. Both phases are highly conductive and band structure calculations indicate the dominant character of the interstack interactions in the conduction process, in contrast to the results obtained for the Ni-based highly conductive phases where intrastack interactions are predominant.

From a qualitative point of view the electrical behavior can be related to the overlap mode of the  $[\text{M}(\text{dmit})_2]$  units. However, no reliable prediction can be made from the sole crystal structure, and band structure calculations are needed to understand the transport properties.

**Acknowledgment.** This work was in part sponsored by CNRS-PIRMAT under Contract "ATP Supraconducteur" No. 89N83/0231. We thank C. Faulmann for conductivity measurements, and D. de Montauzon and J.-B. Tommasino for electrochemical studies. We are indebted to Cristina Tejel for improvement of the synthesis procedures.

**Supplementary Material Available:** Crystallographic data for compounds **2–5** and **7** (Tables S1 and S2), anisotropic thermal parameters for compounds **2–5** and **7** and hydrogen atom parameters for compounds **3** and **7** (Tables S3–S9), electrochemical data for all studied  $(\text{NH}_y\text{Me}_{4-y})[\text{M}(\text{dmit})_2]$  complexes (Table S10), intermolecular S...S distances  $<3.70 \text{ \AA}$  in **2–5**, and **7** (Tables S11–S15), temperature dependent resistivity curve for **2** (Figure SF1), and stacking mode in **5** (Figure SF2) (19 pages). Ordering information is given on any current masthead page.

(47) Doublet, M.-L.; Canadell, E. Unpublished results.

(48) Doublet, M.-L.; Canadell, E.; Pouget, J.-P.; Yagubskii, E. B.; Ren, J.; Whangbo, M.-H. *Solid State Commun.* **1993**, *88*, 699–703.

(49) (a) Whangbo, M.-H.; Ren, J.; Liang, W.; Canadell, E.; Pouget, J.-P.; Ravy, S.; Williams, J. M.; Beno, M. A. *Inorg. Chem.* **1992**, *31*, 4169–4173. (b) Veiros, L. F.; Canadell, E. *J. Phys. I*, in press. (c) Martin, J. D.; Doublet, M.-L.; Canadell, E. *J. Phys. I* **1993**, *3*, 2451–2461. (d) Kahlieh, S.; Schweitzer, D.; Rovira, C.; Paradis, J.; Whangbo, M.-H.; Heinen, I.; Kellen, H. J.; Nuber, B.; Bele, P.; Brunner, H.; Shibaeva, R. *Z. Phys. B, Condensed Mater.*, in press.